

RESEARCH ARTICLE



Comprehensive analysis of the potential mechanism of gansui in blocking non-small cell lung cancer progression

Xiaoxu Yang and Wenlan Li

School of Pharmacy, Harbin University of Commerce, Harbin, Heilongjiang, China

ABSTRACT

Context: Gansui [*Euphorbia kansui* T. N. Liou ex S.B.Ho (Euphorbiaceae)] has been reported to inhibit the proliferation of non-small cell lung cancer (NSCLC) cells; however, its underlying pharmacological mechanism remains unclear.

Objective: To investigate the potential effects and mechanisms of Gansui in blocking NSCLC progression.

Materials and methods: The targets of Gansui's components and NSCLC-related targets were obtained through public database and published studies. Functional enrichment analysis was performed using the clusterProfiler R package. STRING database was used for protein-protein interaction analysis. CytoHubba plugin was applied to get the hub genes. Molecular docking was applied to assess the binding affinities between the hub targets and the crucial components. Kidjolanin was used to treat A549 and NCI-H1385, and its effects on cell viability, sensitivity of paclitaxel and expression levels of hub genes were investigated by cell counting kit-8 assay, flow cytometry and qPCR.

Results: A total of 16 Gansui active ingredients and 337 targets were collected, of which 298 targets overlapped with NSCLC-related genes. *STAT3*, *EGFR*, *GRB2*, *AKT2*, *AKT3* and *PIK3CA* were identified as hub genes. The components in Gansui, including kidjolanin 3-O- β -digitoxopyranoside, cynotophylloside B, 13-Oxyingenol-dodecanoate, and kidjolanin had good binding affinity with the hub targets. Kidjolanin inhibited the viability of NSCLC cells, promoted apoptosis and inhibited the expression of hub genes. Kidjolanin also enhanced the proliferation inhibition and apoptosis of NSCLC cells induced by paclitaxel.

Discussion and conclusion: Gansui exerts anti-NSCLC effects *via* multiple downstream targets, implying its potential in NSCLC treatment.

ARTICLE HISTORY

Received 22 May 2024

Revised 7 December 2024

Accepted 21 February 2025

KEYWORDS

Non-small cell lung cancer; Gansui; network pharmacology; molecular docking

Introduction

Lung cancer is a deadly malignant tumor (Soerjomataram and Bray 2021; Sung et al. 2021). In China, lung cancer ranks the first among the causes of cancer-related death (Wei et al. 2020; Zhang et al. 2022). According to pathology and etiology, lung cancers are mainly divided into two subtypes: non-small cell lung cancer (NSCLC) and small cell lung cancer (SCLC) (Herbst et al. 2018). At present, surgery is considered to be the preferred treatment for early NSCLC (Sun et al. 2020). For the patients with metastasis, a combination of targeted therapy, radiotherapy, chemotherapy and immunotherapy can be adopted (Zhou et al. 2023). However, despite significant advances in treatment, the 5-year survival rate of patients with NSCLC is still unsatisfactory, and the side effects of radiotherapy and chemotherapy seriously reduce patients' quality of life (Lu et al. 2019; Wang et al. 2021). Therefore, there is an urgent need to find new and alternative treatment options.

Gansui is the dried root of *Euphorbia kansui* T. N. Liou ex S.B.Ho (Euphorbiaceae) (Zhang et al. 2019). In China, it is a kind of herbal medicine, and it is also widely used in clinical treatment of edema, ascites, cancer, intestinal obstruction and asthma in traditional Chinese medicine (Zhang et al. 2019). Previous studies have shown that the compounds in Gansui include diterpenoids, triterpenoids, flavonoids, organic acids and organic phenols (Zhang et al. 2017). Among them, diterpenoids (such as kansuine A and B) and triterpenoids (such as euphol)



are the main bioactive components of gansui and the main cause of its toxic effects (Shen et al. 2016). Compared with triterpenoids, diterpenoids of Ganui showed stronger cytotoxic activity (Zhang et al. 2019). A recent study also reports that C21 steroidal glycosides from Gansui also show tumor-suppressive properties (Feng et al. 2023). Modern pharmacological studies have found that Gansui has a wide range of pharmacological activities, such as antiviral, anti-inflammatory, antitumor and immunosuppressive effects (Cheng et al. 2015; Feng et al. 2023). It has been reported that the ethyl acetate extract of Gansui has a significant inhibitory effect on the proliferation of human lung cancer cell A549 (Ma et al. 2016). However, its mechanism of action in the treatment of NSCLC remains unclear.

In this study, we used network pharmacology and molecular docking to predict the main active ingredients, potential targets and affected pathways of Gansui. Finally, the tumor-suppressive functions of kidjolanin, one of the main components of Gansui, were verified using *in vitro* experiments.

Materials and methods

Screening of active components of Gansui and their targets

The key word 'Gansui' was imported into TCMSp database (<https://www.tcmsp-e.com/tcmsp.php>). The potential active ingredients were obtained according to oral bioavailability (OB) \geq 30%

CONTACT Wenlan Li  liwlhlj@sina.com  School of Pharmacy, Harbin University of Commerce, Harbin 150001, Heilongjiang, China.

© 2025 The Author(s). Published by Informa UK Limited, trading as Taylor & Francis Group.

This is an Open Access article distributed under the terms of the Creative Commons Attribution-NonCommercial License (<http://creativecommons.org/licenses/by-nc/4.0/>), which permits unrestricted non-commercial use, distribution, and reproduction in any medium, provided the original work is properly cited. The terms on which this article has been published allow the posting of the Accepted Manuscript in a repository by the author(s) or with their consent.

and drug similarity (DL) ≥ 0.18 (Xiang et al. 2022; Qian and Yi 2024). In addition, based on previous studies (Feng et al. 2023; Wang et al. 2024), additional potential active ingredients were obtained. PubChem database (<https://pubchem.ncbi.nlm.nih.gov/>) and NovoPro online platform (<https://novopro.cn/tools/mol2smiles.html>) were used for obtaining the SMILES format file of the ingredients. Then SwissTargetPrediction database (<http://www.swisstargetprediction.ch/>) was searched to predict the potential targets of active ingredients. Probability > 0 was used as the screening criterion. Cytoscape 3.9.0 software was used to construct the ‘components - targets’ network of Gansui.

Screening and collection of NSCLC - related targets

‘Non-small cell lung cancer’ was selected as the search term in the Comparative Toxicogenomics Database (CTD) (<https://ctdbase.org/>; inference score ≥ 10), GeneCards database (relevance score ≥ 10 , category: Protein coding) (Li et al. 2022) and DisGeNET database (<https://www.disgenet.org/>) were searched for predicting NSCLC - related target genes. After integrating the retrieved targets and deleting the duplicates, NSCLC-related target genes were obtained.

Screening of the targets of Gansui in NSCLC treatment

Gansui's target genes and NSCLC - related targets were imported to BioLadder online platform (https://bioinfo.gp.cnb.csic.es/tools/venny_old/), to get the intersection of the two gene sets.

Functional annotation of gene ontology (GO) and enrichment analysis of Kyoto Encyclopedia of Genes and Genomes (KEGG) pathways

GO and KEGG enrichment analyses on target genes were performed using the R package clusterProfiler. $p < 0.05$ was the significance threshold.

Construction of protein-protein interaction (PPI) network

PPI network analysis of intersection targets was performed using STRING database (<https://cn.string-db.org/>). The species was set as ‘homo sapiens’, and the required minimum interaction score was set as ‘highest confidence (0.900)’. After removing the free points, PPI network was obtained, and TSV file was downloaded and saved. The Molecular Complex Detection (MCODE) plug-in was then used to screen important modules in the PPI network, with the criteria as follows: degree cutoff = 2, node score cutoff = 0.2, K-score = 2 and max depth = 100.

Identification and analysis of hub genes

With CytoHubba plug-in in Cytoscape 3.9.0 software, different algorithms including ‘betweenness’, ‘closeness’, ‘edge percolated component (EPC)’, ‘degree’, ‘maximal clique centrality (MCC)’, ‘maximum neighborhood component (MNC)’, ‘radiality’ and ‘stress’, were calculated to obtain the top 30 genes in the PPI network. Further, R package UpSet was applied to screen the hub genes. Then, the co-expression network of hub genes and their co-expressed genes was constructed based on GeneMANIA (<http://genemania.org/>). In addition, KEGG analysis of hub genes were performed using the clusterProfiler package of R software.

Immune infiltration analysis

Tumor Immune Estimation Resource (TIMER) database (<https://cistrome.shinyapps.io/timer/>) was used to analyze the relationship between hub gene expression and NSCLC immune cell infiltration.

Construction and analysis of ‘component - hub gene - pathway’ network

Cytoscape 3.9.0 software was used to construct the ‘component-hub gene - pathway’ network diagram, and CytoNCA plug-in was used to calculate the degree value of network nodes, to screen out the key chemical components and signaling pathways of Gansui for the treatment of NSCLC.

Molecular docking

PubChem database (<https://pubchem.ncbi.nlm.nih.gov/>) was searched to download the 2D structure of the key ingredients. X-ray crystal structures of hub proteins were downloaded from Protein Data Bank (PDB) database (<https://www.rcsb.org/>). Protein hydrogenation and charge calculation were performed with AutoDockTools (version 1.5.7). In addition, AutoDockTools (version 1.5.7) was applied to set key compounds as ligands, and then AutoDock Vina (version 1.1.2) was applied to perform molecular docking. Binding energy < 0 indicates that the ligand had the potential to spontaneously bind to the receptor (Long et al. 2022). Finally, PyMol (version 2.4.0) software was used to visualize the docking results, which were displayed as 3D diagrams.

Cell culture and preparation of kidjolanin solution

Human NSCLC cell lines A549 (CCL-185; CVCL_0023; *Homo sapiens*) and NCI-H1385 (CRL-5867; CVCL_1466; *Homo sapiens*) were purchased from American Type Culture Collection (ATCC, Manassas, VA, USA). The cells were placed in a petri dishes containing Dulbecco's Modified Eagle's Medium (DMEM; MBS2557643-E; Gibco, Carlsbad, CA, USA) with 10% fetal bovine serum (FBS; C0234; Beyotime, Shanghai, China), 100 U/mL penicillin and 100 μ g/mL streptomycin (C0222; Beyotime, Shanghai, China) and cultured at 37°C and 5% CO₂. Kidjolanin (38395-01-6, Cuiyuan Biotech, Wuhan, China) was then dissolved in dimethylsulfoxide (DMSO; D2650; Sigma-Aldrich, Shanghai, China) and diluted by the medium and filtered by 0.22 μ m filter twice.

Cell viability assay

To investigate the effects of kidjolanin on NSCLC cell viability, the cells were inoculated into 96-well plates at a density of 3×10^4 cells per well and cultured overnight. Then the cells were treated with different concentrations (0, 20, 40, 60, 80, 100 μ M) of kidjolanin for 24 h. Next, the supernatant was removed and the DMEM (without FBS) containing 10 μ L of cell counting kit-8 (CCK-8) (C0037; Beyotime, Shanghai, China) was added to each well. After incubation at 37°C for 1 h, the absorbance was measured at 460 nm wavelength using a microplate reader. The half maximal inhibitory concentration (IC₅₀) of kidjolanin on A549 and NCI-H1385 cells at 24 h was determined. To investigate the synergistic tumor-suppressive effects of kidjolanin and paclitaxel,

the NSCLC cells were inoculated into 96-well plates at a density of 3×10^4 cells/well and treated with different concentrations (0, 1.25, 2.5, 5, 10 and 20 $\mu\text{g/mL}$) of paclitaxel (580555; Sigma-Aldrich, Shanghai, China) for 48 h in the presence or absence of 60 μM kidjolanin. The cells treated with DMSO (Sigma-Aldrich, Shanghai, China) were used as the negative controls.

Flow cytometry

An Annexin V-Fluorescein Isothiocyanate (FITC)/propidium iodide (PI) apoptosis detection kit (C1062S; Beyotime, Shanghai, China) was used to detect apoptosis. A549 and NCI-H1385 cells at the logarithmic growth stage were inoculated in a 6-well plate (4×10^5 cells/well), incubated overnight at 37°C. Then the cells were treated with different concentrations (0, 20 and 60 μM) of kidjolanin for 24 h, or treated with 10 $\mu\text{g/mL}$ paclitaxel (Sigma-Aldrich, Shanghai, China) for 48 h in the presence or absence of 60 μM kidjolanin. The cells treated with DMSO (Sigma-Aldrich, Shanghai, China) were used as the negative controls. The harvested cells were washed with phosphate buffered saline (PBS) (C0221A; Beyotime, Shanghai, China) and then re-suspended in the binding buffer. Next, the cells were incubated at room temperature with 5 μL of Annexin V-FITC and 5 μL of PI for 15 min away from light. The stained cells were then analyzed with a FACScan flow cytometer (BD Biosciences, Franklin Lakes, NJ, USA) and the results were analyzed by FlowJo V.10 software. Gating strategy was based on forward scatter signal and side scatter signal, to exclude the influence of cell mass and cell debris on the result analysis.

Quantitative real-time polymerase chain reaction (qRT-PCR) assay

TRIzol reagent (NR0046; Invitrogen, Carlsbad, CA, USA) was used to extract total RNA. Complementary DNA (cDNA) was synthesized using a PrimeScript RT kit (RR037B; TaKaRa, Dalian, China). The reaction condition: 25°C for 5 min, 50°C for 15 min, 85°C for 5 min. After obtaining the cDNA, qRT-PCR was performed using a SYBR Premix Ex Taq kit (DRR041A; TaKaRa, Dalian, China) in Applied Biosystems System 7500 (Thermo Fisher Scientific, Waltham, MA, USA). The reaction condition of PCR: 94°C for 40 s, 55°C for 40 s, 72°C for 40 s for 45 cycles. Aldehyde -3-phosphate dehydrogenase (*GAPDH*) was used as the internal control, and the relative expression of target genes was calculated by $2^{-\Delta\Delta C_t}$. The specific primers' sequences for qRT-PCR were as follows: signal transducer and activator of transcription 3 (*STAT3*): 5'-TGTGCATTGACAATCTGTGTTCT-3' (forward) and 5'-TGGAGATCACCACAACCTGGC-3' (reverse); epidermal growth factor receptor (*EGFR*): 5'-TTGCCGCAAAGTGTGTAACG-3' (forward) and 5'-AGGGAACAGGAAATATGTCGAA-3' (reverse); growth factor receptor-bound protein 2 (*GRB2*): 5'-ACGACGAGCTGAGCTTCAA-3' (forward) and 5'-CGTTTCCAAACGGATGTGGTT-3' (reverse); RAC-beta serine/threonine-protein kinase (*AKT2*): 5'-CTGCCACCATGAATGAGGTGAA-3' (forward) and 5'-CATGGTCACTTTAGCCCGTG-3' (reverse); RAC-gamma serine/threonine-protein kinase (*AKT3*): 5'-TTTTCTCTATTATTGGGCTGAGTC-3' (forward) and 5'-CCCCTCTTCTGAACCCAACC-3' (reverse); phosphatidylinositol 4,5-bisphosphate 3-kinase catalytic subunit alpha isoform (*PIK3CA*): 5'-GGACCCGATGCGGTTAGAG-3' (forward) and 5'-ATCAAGTGGATGCCCCACAG-3' (reverse); *GAPDH*: 5'-GAAGGTGAAGTCCGAGTC-3' (forward) and 5'-GAAGATGGTGATGGGATTC-3' (reverse).

Statistical analysis

For the *in vitro* assays, all experiments were conducted independently in triplicate. All data were expressed as 'mean \pm standard deviation (SD)'. SPSS 21.0 software (IBM Corp., Armonk, NY, USA) was used for statistical analysis of the data. The data in multiple groups were compared using one-way analysis of variance (ANOVA) and Tukey *post hoc* test. A *p* value <0.05 was considered statistically significant.

Results

Screening of active ingredients and the targets of Gansui

According to the screening criteria of OB $\geq 30\%$ and DL ≥ 0.18 , a total of 8 potential bioactive ingredients of Gansui were identified from TCMSP database. In addition, 13 ingredients of Gansui were obtained through previous reports (Feng et al. 2023; Wang et al. 2024) (Table 1). PubChem database was used to obtain the 2D chemical structures and SMILES files of these components. Due to the lack of the information of eupokanu G, cynsacatol L, kidjoranin-3-O- β -D-cymaropyranoside, cynophylloside J and caudatin 3-O- β -D-digitoxopyranoside in PubChem database, they were removed. Then the potential targets of these components were predicted by the SwissTargetPrediction database according to the screening criteria with probability > 0, and a total of 337 drug targets were finally obtained. Then Gansui's component-target network with 351 nodes and 698 edges was constructed using Cytoscape 3.9.0 software (Figure 1).

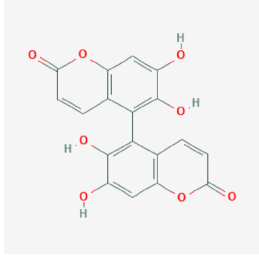
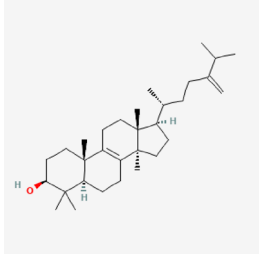
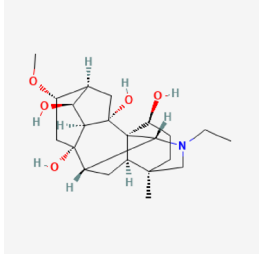
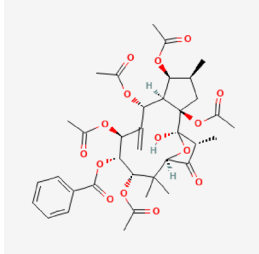
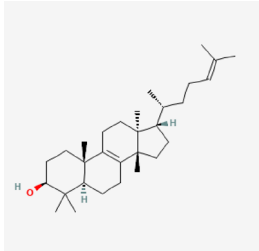
Collection of the target genes of Gansui associated with NSCLC progression

Disease target genes associated with NSCLC were searched using the CTD, GeneCards and DisGeNET databases, and 9350, 4003 and 65 NSCLC-related genes were obtained, respectively (Figure 2(A)). After combining these gene targets and removing the duplicate targets, a total of 10,481 NSCLC-related disease targets were finally identified. To obtain potential targets for the treatment of NSCLC, 377 drug targets were cross analyzed with 10,481 disease targets. The results showed that 298 targets were identified as potential candidates for the treatment of NSCLC with Gansui (Figure 2(B)).

GO analysis and KEGG enrichment analysis of Gansui target genes in NSCLC treatment

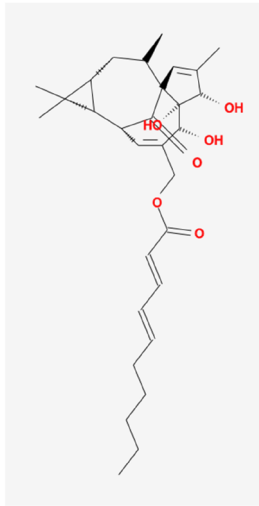
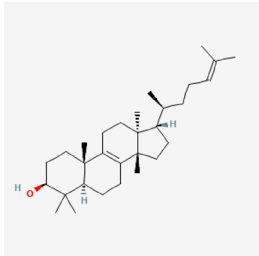
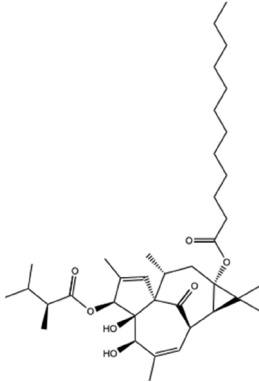
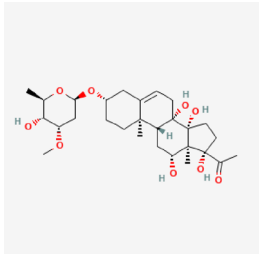
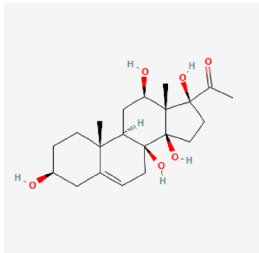
To explore the potential functional mechanisms of Gansui in NSCLC, we used the R software package clusterProfiler to perform GO analysis and KEGG pathway enrichment analysis for 298 drug-disease targets. The results showed that a total of 2925 GO items were enriched in the potential targets of Gansui for NSCLC treatment, including 2528 biological processes (BP), 150 cell components (CC) and 247 molecular functions (MF). We selected the top 10 BP, CC and MF items with the smallest *p* values, respectively, for visualization. As shown, for BP, in lung cancer treatment, Gansui was mainly associated with peptidyl-serine phosphorylation, peptidyl-serine modification, rhythmic process, regulation of small molecule metabolic process and positive regulation of protein transport, etc. (Figure 3(A)). For CC, Gansui in NSCLC treatment was also associated with serine/threonine protein kinase complex, protein kinase complex, cyclin-dependent protein kinase holoenzyme complex, transferase

Table 1. Details of active compounds in Gansui.

No.	Name	PubChem CID	MW (g/mol)	SMILES	Target	Structure
1	Euphorbetin	5317297	354.3	<chem>C1=CC(=O)OC2=C1C(=C(C(=C2)O)O)C3=C(C(=CC4=C3C=CC(=O)O4)O)O</chem>	15	
2	Eburicol	9803310	440.7	<chem>CC(C)C(=C)CCC(C)C1CCC2(C1(CCC3=C2CCC4C3(CCC(C4(C)C)O)C)C)C</chem>	53	
3	Karacolidine	101306844	393.5	<chem>CCN1CC2(CCC(C34C2CC(C31)C5(CC(C6CC4(C5C6O)O)OC)O)O)C</chem>	18	
4	Kansuinin A	11366139	730.8	<chem>CC1CC2(C(C1OC(=O)C)C(C(=C)C(C(C(C3C(=O)C(C2(O3)O)C)C)OC(=O)C)OC(=O)C4=CC=CC=C4)OC(=O)C)OC(=O)C)OC(=O)C</chem>	14	
5	Euphol	441678	426.7	<chem>CC(CCC=C(C)C)C1CCC2(C1(CCC3=C2CCC4C3(CCC(C4(C)C)O)C)C)C</chem>	58	

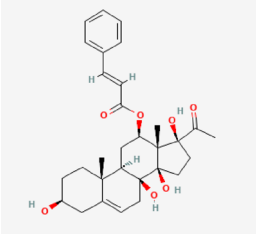
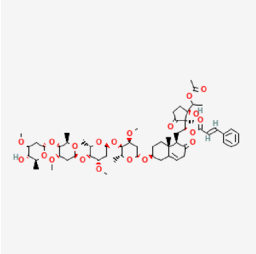
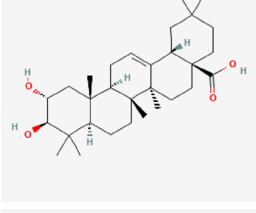
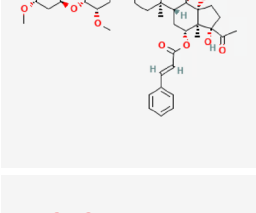
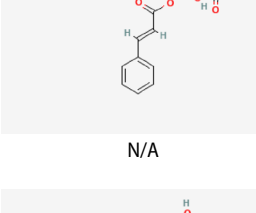

(Continued)

Table 1. Continued.

No.	Name	PubChem CID	MW (g/mol)	SMILES	Target	Structure
6	20-OD-ingenol Z	N/A	498.7	<chem>CCCCC=CC=CC(=O)OCC1=C[C@H]2C(=O)[C@]3(C=C(C)[C@H](O)[C@@]3(O)[C@@H]1O)[C@H](C)C[C@@H]1[C@H]2C1(C)C</chem>	112	
7	Kanzuol	101257	426.7	<chem>CC(CCC=C(C)C)C1CCC2(C1(CCC3=C2CCC4C3(CCC(C4(C)C)O)C)C)C</chem>	58	
8	3-O-(2,3-Dimethylbutanoyl)-13-O-dodecanoyl-20-deoxyingenol	N/A	629.0	<chem>CCCCCCCCCCC(=O)O[C@@]12C[C@@H](C)[C@]34C=C(C)[C@H](OC(=O)[C@@H](C)C(C)C)[C@@]3(O)[C@H](O)C(C)=C[C@@H](C4=O)[C@@H]1C2(C)C</chem>	27	
9	Eupokanu G	N/A	N/A	N/A	N/A	N/A
10	Cynotophylloside B	101556123	524.6	<chem>CC1C(C(CC(O1)OC2CCC3(C4CC(C5(C(CCC5(C4(CC=C3C2)O)O)(C(=O)C)O)C)O)C)OC)O</chem>	39	
11	Deacylmetaplexigenin	21633061	380.5	<chem>CC(=O)C1(CCC2(C1(C(CCC2(C=C4C3(CCC(C4)O)C)O)C)O)C)O)O</chem>	0	

(Continued)

Table 1. Continued.

No.	Name	PubChem CID	MW (g/mol)	SMILES	Target	Structure
12	Kidjolanin	21633060	510.6	<chem>CC(=O)C1(CCC2(C1(C(C3C2(CC=C4C3(CCC(C4)O)C)O)OC(=O)C=CC5=CC=CC=C5)C)O)O</chem>	108	
13	Cynsaccatol L	N/A	N/A	N/A	N/A	N/A
14	Kidjoranin-3-O-β-D-cymaropyranoside	N/A	N/A	N/A	N/A	N/A
15	Wilfoside G	102165354	1129.3	<chem>CC1C(C(C(C(OC2C(OC(C2OC)OC3C(OC(C3OC)OC4C(OC(C4OC)OC5CCC6(C(C(=O)CC=C6C5)CC(C7(C(=O)CCC7(C(C(=O)C)O)C)OC(=O)C=CC8=CC=CC=C8)C)C)C)OC)O</chem>	8	
16	Cynotophylloside J	N/A	N/A	N/A	N/A	N/A
17	Maslinic acid	73659	472.7	<chem>CC1(CCC2(CCC3(C(=CCC4C3(CCC5C4(CC(C(C5(C)O)O)C)C)C2C1)C(=O)O)C</chem>	75	
18	Kidjoranin 3-O-α-diginopyranosyl-(1→4)-β-cymaropyranoside	70697805	799.0	<chem>CC1C(C(C(C(OC2C(OC(C2OC)OC3CCC4(C5CC(C6(C(CCC6(C5(CC=C4C3)O)O(C(=O)C)O)C)OC(=O)C=CC7=CC=CC=C7)C)C)OC)O</chem>	0	
19	Kidjoranin 3-O-β-digitoxopyranoside	70697800	640.8	<chem>CC1C(C(C(C(OC2CCC3(C4CC(C5(C(CCC5(C4(CC=C3C2)O)O(C(=O)C)O)C)OC(=O)C=CC6=CC=CC=C6)C)O)O</chem>	52	
20	Caudatin 3-O-β-D-digitoxopyranoside	N/A	N/A	N/A	N/A	N/A
21	13-Oxyingenol-dodecanoate	85364165	546.7	<chem>CCCCCCCCCCCC(=O)OC12CC(C34C=C(C(C3(C(C(=CC(C1C2(C)C)C4=O)CO)O)O)C)C</chem>	61	

Note: MW: molecular weight; N/A: not applicable.

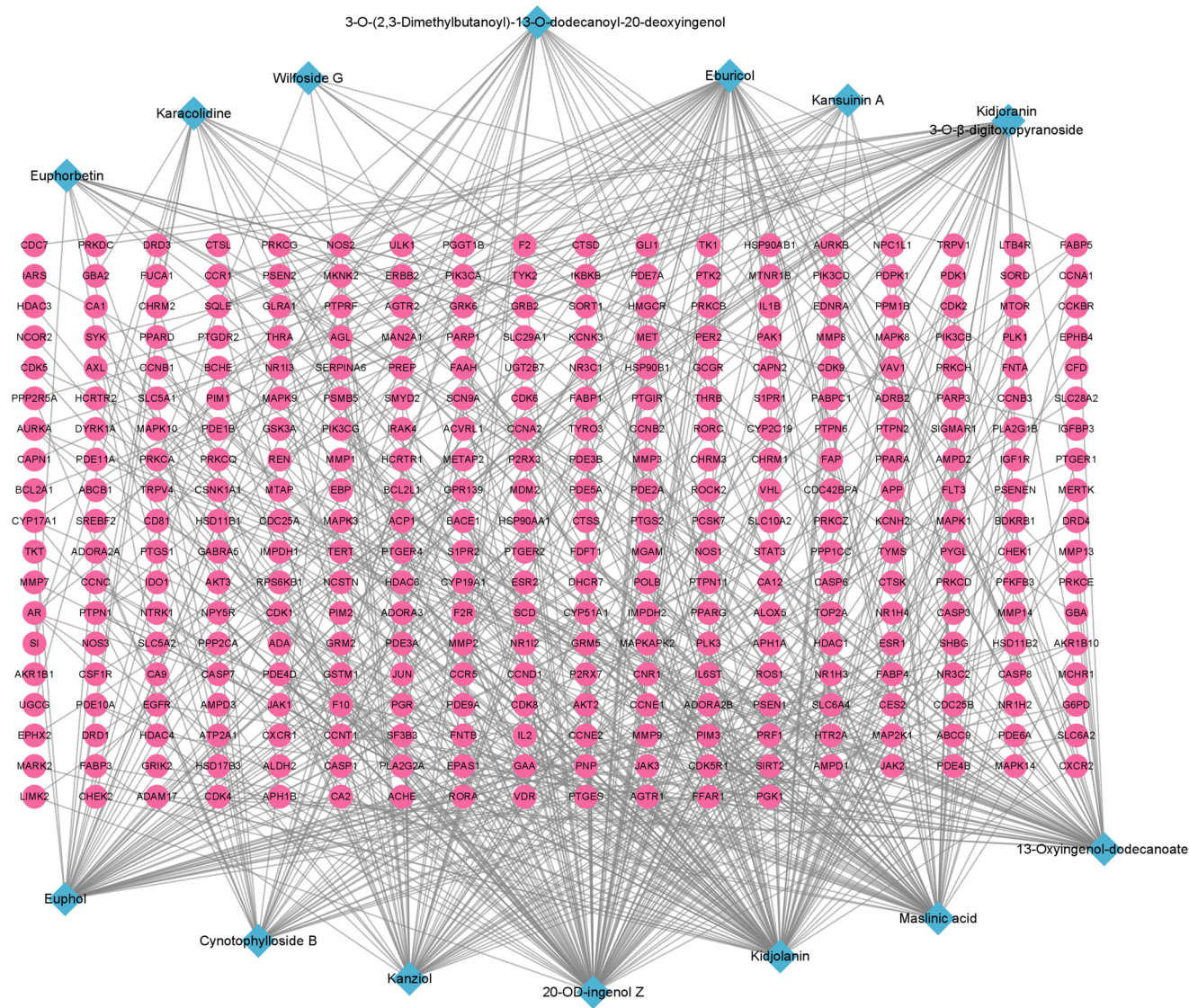


Figure 1. The ‘components - targets’ network of Gansui. Pink circular nodes represent targets and blue diamond nodes represent components.

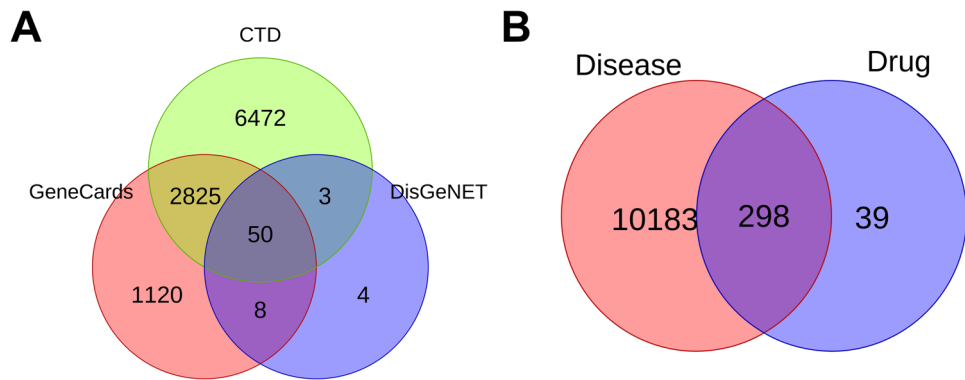


Figure 2. Screening of potential targets for Gansui in treatment of NSCLC. (A) Venn diagram of NSCLC-related disease targets in CTD, GeneCards and DisGeNET databases. (B) Venn diagram of Gansui targets and NSCLC-related gene targets.

complex, transferring phosphorus-containing groups and membrane raft, etc. (Figure 3(B)); for MF, it was associated with protein serine/threonine kinase activity, nuclear receptor activity, ligand-activated transcription factor activity, protein tyrosine kinase activity and steroid binding, etc. (Figure 3(C)). In addition, through KEGG enrichment analysis, 168 pathways were

found to be probably associated with Gansui in the treatment of NSCLC. We then selected the top 10 KEGG pathways with the smallest *P*-values for visualization. The results showed that the targets of Gansui in NSCLC treatment were mainly enriched in endocrine resistance, acute myeloid leukemia, AGE-RAGE signaling pathway in diabetic complications, prostate cancer, insulin

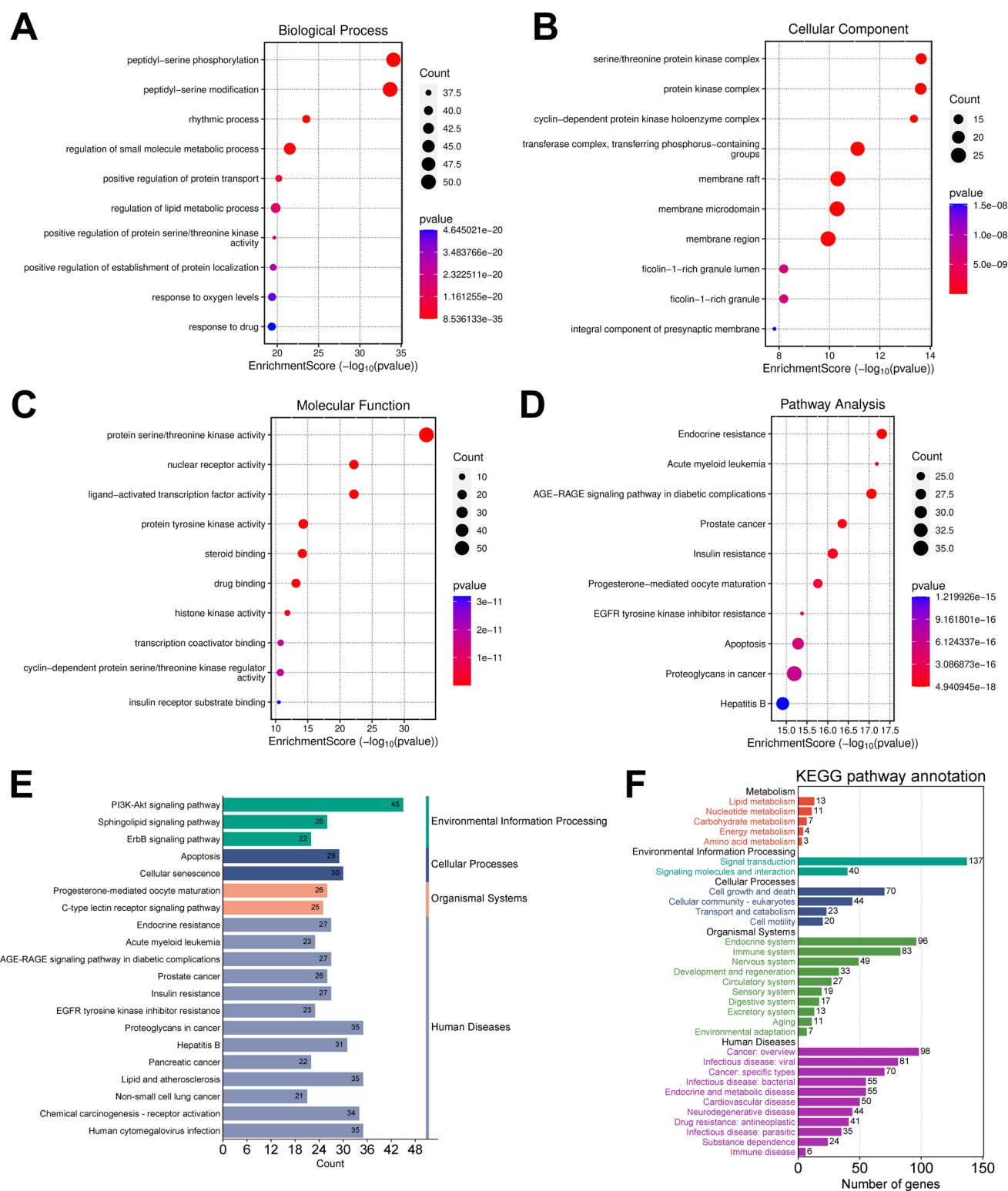


Figure 3. GO analysis and KEGG enrichment analysis of the common targets. (A–D) Bubble map was used to show the BP (A), CC (B), MF (C) and KEGG pathway (D) probably modulated by the targets of Gansui associated NSCLC. The vertical and horizontal axes show the items names and the enrichment score, respectively. The color and size of the bubbles represent *p* values and gene counts, respectively. (E) Classification summary diagram of the top 20 KEGG pathways. (F) Secondary classification diagram of the pathways associated with Gansui's targets in NSCLC treatment (168 in total).

resistance, progesterone-mediated oocyte maturation, *EGFR* tyrosine kinase inhibitor resistance, apoptosis, proteoglycans in cancer, hepatitis B (Figure 3(D)). Further, we classified and summarized the top 20 KEGG pathways. It was found that these KEGG pathways were mainly divided into four categories, including environmental information processing, cellular processes,

organismal systems and human diseases (Figure 3(E)). In addition, we conducted a secondary classification of all KEGG pathways. The results showed that KEGG pathways were mainly about lipid metabolism, signal transduction, cell growth and death, endocrine system, immune system, cancer, etc. (Figure 3(F)).

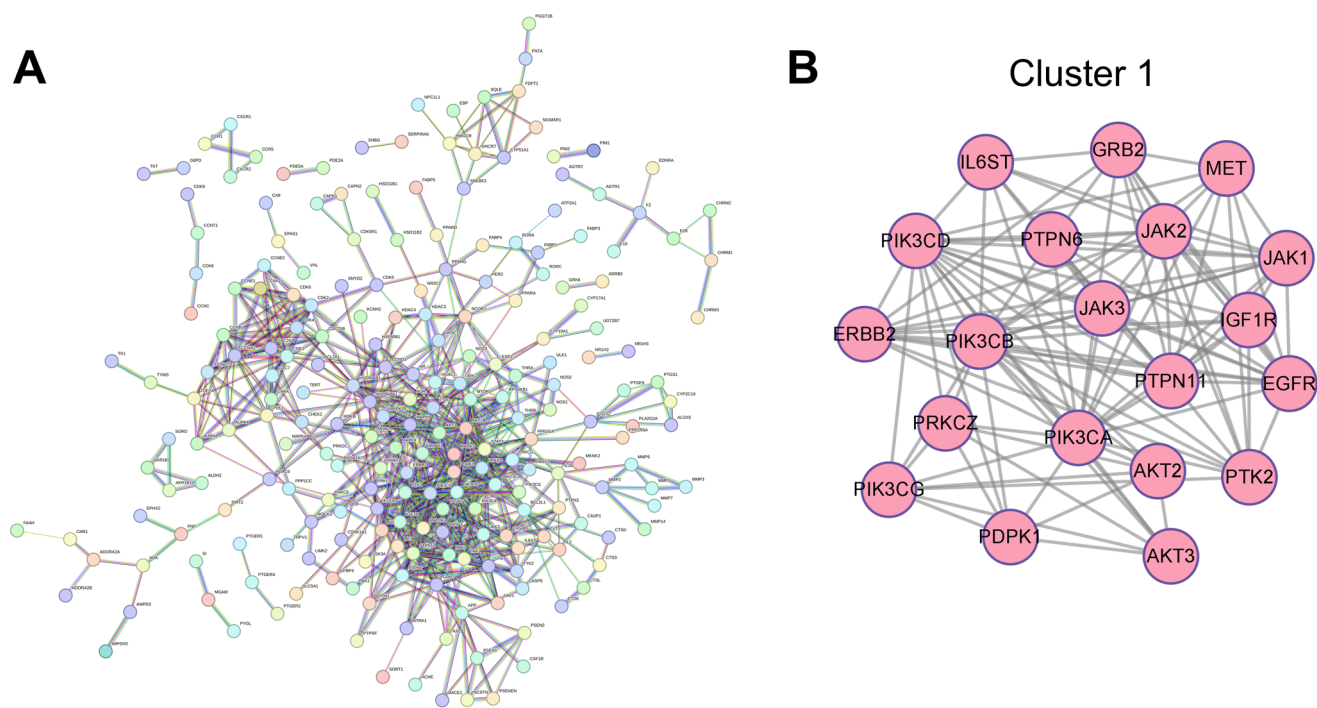


Figure 4. Construction of PPI network based on the targets of Gansui in the treatment of NSCLC. (A) PPI network of the targets of Gansui in NSCLC treatment. (B) The PPI network was analyzed using the MCODE plug-in to get a cluster 1 with the highest score.

Table 2. Clusters of target genes of gansui against non-small cell lung cancer.

Cluster	Score (density*#nodes)	Nodes	Edges	Node IDs
1	11.684	20	111	PTK2, IGF1R, PIK3CD, PIK3CB, PTPN6, JAK2, PIK3CG, JAK1, PTPN11, AKT3, AKT2, PIK3CA, JAK3, EGFR, IL6ST, MET, GRB2, PDPK1, ERBB2, PRKCZ
2	6.923	14	45	PRKCB, RPS6KB1, MAPK8, PRKCD, MAPK9, JUN, PPP2CA, STAT3, MAPK1, MTOR, PRKCG, MAPK3, PRKCA, CASP3
3	6	10	27	CCNA1, CCNB1, CDK6, TOP2A, PLK1, AURKB, CDK4, CDK1, CCNB2, AURKA
4	5	5	10	FDFT1, DHCR7, SQLE, CYP51A1, HMGCR
5	5	5	10	PSEN1, NCSTN, APP, PSEN2, PSENEN
6	4	4	6	CYP2C19, PTGS1, ALOX5, PTGS2
7	3.333	4	5	CCNA2, CCNE1, CDK2, CCNE2
8	3.333	4	5	MMP2, MMP1, MMP3, MMP9
9	3.333	4	5	ALDH2, AKR1B1, SORD, AKR1B10
10	3	3	3	NOS2, NOS3, NOS1
11	3	3	3	NCOR2, HDAC1, NR3C1
12	3	3	3	ESR1, PGR, HSP90AB1
13	3	3	3	CHRM1, CHRM2, F2R
14	3	3	3	CAPN1, CDK5R1, CAPN2
15	2.667	4	4	CCR1, CXCR1, CXCR2, CCR5

PPI network construction and analysis

The 298 related target genes were then imported into STRING database to construct PPI network. The network consisted 226 nodes and 698 edges with an average node degree of 4.68 and an average local clustering coefficient of 0.43 (Figure 4(A)). In addition, MCODE analysis of this network was performed to further investigate the intrinsic connectivity of these targets, and 15 important clusters were found (Table 2), and cluster 1 was with the highest score, with 20 nodes and 111 edges (Figure 4(B)).

Identification of hub target genes

Next, the parameters of the top 30 key genes of the PPI network were calculated using the cytoHubba plug-in (Table 3). Next, the hub genes in the intersection were obtained, and the results showed that *STAT3*, *EGFR*, *GRB2*, *AKT2*, *AKT3* and *PIK3CA* were the hub genes (Figure 5(A)). All of the hub genes were also in cluster 1 (Figure 5(B)), further suggesting that these 6 genes were crucial in the PPI network, and they synergistically promoted disease progression. Detailed information of these six hub genes is shown in Table 4. In addition, based on the GeneMANIA database, we analyzed the co-expression networks of hub genes, which exhibited these hub genes were significantly interacted with each other. Physical interaction accounted for 48.72%, co-expression accounted for 5.28%, pathway accounted for 10.61%, prediction accounted for 29.54%, co-localization accounted for 2.39% and shared protein domain accounted for 3.46% (Figure 5(B)). KEGG pathway analysis showed that hub genes were mainly associated with EGFR tyrosine kinase inhibitor resistance, neurotrophin signaling pathway, ErbB signaling pathway, insulin signaling pathway, proteoglycans in cancer, non-small cell lung cancer, glioma, chronic myeloid leukemia and growth hormone synthesis, secretion and action (Figure 5(C)).

The expression of hub genes is related with the infiltration of immune cells in NSCLC tissues

To investigate the relationship between the expression level of hub gene and the level of immune infiltration in NSCLC tissues, TIMER database was searched. The results are shown in Figure 6. We found that *STAT3* expression levels in lung adenocarcinoma (LUAD) and lung squamous cell carcinoma (LUSC) were positively correlated with infiltration of B cells, CD8+T cells, CD4+T cells, macrophages, neutrophils and dendritic cells but negatively correlated with tumor purity in LUSC. *EGFR* expression was positively correlated with the infiltration levels of B

Table 3. The top 30 gene rank in cytoHubba.

No.	Betweenness	Closeness	Degree	EPC	MCC	MNC	Radiality	Stress
1	STAT3	STAT3	PIK3CA	PIK3CA	PIK3CA	PIK3CA	STAT3	HSP90AA1
2	HSP90AA1	HSP90AA1	STAT3	PIK3CB	PTPN11	PIK3CD	HSP90AA1	STAT3
3	PPARG	MAPK1	PIK3CD	PIK3CD	JAK2	PIK3CB	ESR1	PPARG
4	HDAC6	ESR1	PIK3CB	STAT3	PIK3CD	STAT3	MAPK1	SREBF2
5	SREBF2	AKT2	MAPK1	PTPN11	PIK3CB	MAPK1	AKT2	MTOR
6	MTOR	AKT3	HSP90AA1	EGFR	EGFR	PTPN11	AKT3	NCOR2
7	SIRT2	EGFR	PTPN11	MAPK1	JAK1	AKT2	EGFR	GRB2
8	EGFR	PIK3CA	EGFR	AKT3	ERBB2	AKT3	JUN	MAPK1
9	PNP	JUN	AKT2	AKT2	JAK3	ESR1	MTOR	EGFR
10	JUN	PTPN11	AKT3	ESR1	IGF1R	MAPK3	HSP90AB1	HDAC6
11	MAPK1	MAPK3	ESR1	ERBB2	PTK2	EGFR	ERBB2	ESR1
12	ADA	PIK3CD	MAPK3	JAK2	PTPN6	HSP90AA1	PIK3CA	CCND1
13	NCOR2	PIK3CB	GRB2	MAPK3	MET	JAK2	CCND1	JUN
14	GRB2	ERBB2	JAK2	HSP90AA1	CCNA2	HSP90AB1	AR	APP
15	ESR1	HSP90AB1	HSP90AB1	GRB2	GRB2	GRB2	PTPN11	SIRT2
16	CASP3	MTOR	JAK1	PTK2	CDK1	JAK1	MAPK3	PIK3CA
17	NR3C1	GRB2	JUN	JAK1	IL6ST	ERBB2	PGR	CDK1
18	PTGS2	JAK2	ERBB2	IGF1R	CCNB1	CDK1	PIK3CD	AKT2
19	CDK5	MAPK8	CDK1	PTPN6	AKT2	CCNA2	PIK3CB	AKT3
20	BCL2L1	PTK2	PTK2	JAK3	AKT3	PTPN6	NR3C1	CASP3
21	CCND1	IGF1R	CASP3	JUN	PLK1	CDC25A	MAPK8	PNP
22	APP	CCND1	CCNA2	MTOR	CCNB2	IGF1R	MDM2	HSP90AB1
23	HSP90AB1	MAPK14	PTPN6	HSP90AB1	PRKCZ	JUN	IGF1R	NR3C1
24	AKT2	MDM2	MAPK14	MAPK14	PIK3CG	PTK2	PTK2	PIK3CD
25	AKT3	PGR	CDC25A	MET	PDPK1	MAPK8	MAPK14	PIK3CB
26	CDK1	CASP3	IGF1R	PRKCD	AURKB	JAK3	JAK2	ERBB2
27	MMP2	BCL2L1	NCOR2	IL6ST	AURKA	CASP3	HDAC1	ADA
28	PIK3CA	JAK1	MAPK8	PGR	TOP2A	CCNB1	ESR2	CDK5
29	ADORA2A	AR	JAK3	MAPK8	STAT3	CDK2	GRB2	CDK4
30	IL1B	PTPN6	CDK2	PRKCZ	CDC25A	PLK1	BCL2L1	BCL2L1

cells, CD8+T cells, CD4+T cells, neutrophils and dendritic cells in LUAD, as well as CD4+T cells in LUSC, while negatively correlated with the infiltration levels of B cells and CD8+T cells in LUSC. The expression of *GRB2* was positively correlated with the infiltration levels of B cells, CD8+T cells, CD4+T cells, macrophages, neutrophils and dendritic cells in LUAD, as well as B cells, CD4+T cells, macrophages, neutrophils and dendritic cells in LUSC, while negatively correlated with the infiltration levels of purity in LUAD and LUSC. The expression of *AKT2* was positively correlated with the infiltration levels of CD4+T cells, macrophages, neutrophils and dendritic cells in LUAD, as well as CD4+T cells, macrophages and neutrophils in LUSC. The expression of *AKT3* was positively correlated with the infiltration levels of B cells, CD8+T cells, CD4+T cells, macrophages, neutrophils and dendritic cells in LUAD and LUSC, but negatively correlated with the infiltration level of purity in LUAD. The expression of *PIK3CA* was positively correlated with the infiltration levels of CD8+T cells, CD4+T cells, macrophages, neutrophils, dendritic cells and purity in LUAD and LUSC, but negatively correlated with the infiltration levels of neutrophils in LUSC. These results suggest that there was a significant correlation between hub gene expression and immune cell infiltration in NSCLC, implying that Gansui may modulate the immune microenvironment of NSCLC.

Construction and analysis of 'component - hub gene - pathway' network

The 'component - hub gene - pathway' network was constructed using Cytoscape 3.9.0 to further screen the key components and pathways of Gansui in NSCLC treatment. The network consisted of 30 nodes and 102 edges (Figure 7(A)). The size of a node was proportional to its degree value in the network. The degree values of the network nodes were shown (Figure 7(B)). Kidjoranin 3-O- β -digitoxopyranoside (K3OBD, degree = 3), cynotophylloside

B (CB, degree = 3), 13-oxyingenol-dodecanoate (13OD, degree = 2) and kidjolanin (degree = 2) were considered to be key components of Gansui in the treatment of NSCLC.

Molecular docking analysis

Next, molecular docking was performed to verify the binding ability of the hub proteins and key components of Gansui. K3OBD could form two hydrogen bonds with the amino acid residue ARG-215 of STAT3 protein; CB formed two hydrogen bonds with the amino acid residue ARG-215 of STAT3 protein; 13OD formed one hydrogen bond with the amino acid residue GLU-324 of STAT3 protein. Kidjolanin formed two hydrogen bonds with the amino acid residues GLN-326 and GLN-247 of STAT3 protein; the STAT3 inhibitor (AG490) could form three hydrogen bonds with the amino acid residues SER-540 and TYR-539 of STAT3 protein (Figure 8(A)). K3OBD formed one hydrogen bond with amino acid residue LYS-875 of EGFR protein; CB formed two hydrogen bonds with amino acid residues ALA-722 and ARG-841 of EGFR protein; 13OD formed three hydrogen bonds with amino acid residues SER-720 and ASN-842 of EGFR protein, kidjolanin formed two hydrogen bonds with amino acid residues ASN-842 and LEU-718 of EGFR protein, and EGFR inhibitor afatinib could form one hydrogen bond with amino acid residue LEU-718 of EGFR protein (Figure 8(B)). K3OBD, CB and kidjolanin could each form one hydrogen bond with the amino acid residue LEU-120 of GRB2 protein, 13OD formed a hydrogen bond with the amino acid residue TRP-121 of GRB2 protein, GRB2 inhibitor lymecycline could form 8 hydrogen bonds with the amino acid residues VAL-123, TYR-134, HIS-135, SER-139 and SER-141 of GRB2 protein (Figure 8(C)). K3OBD formed five hydrogen bonds with amino acid residues VAL-272, ASN-53, ARG-23 and ASP-324 of AKT2 protein; CB formed one hydrogen bond with amino acid residue GLU-59 of AKT2 protein; 13OD formed three hydrogen bonds with amino

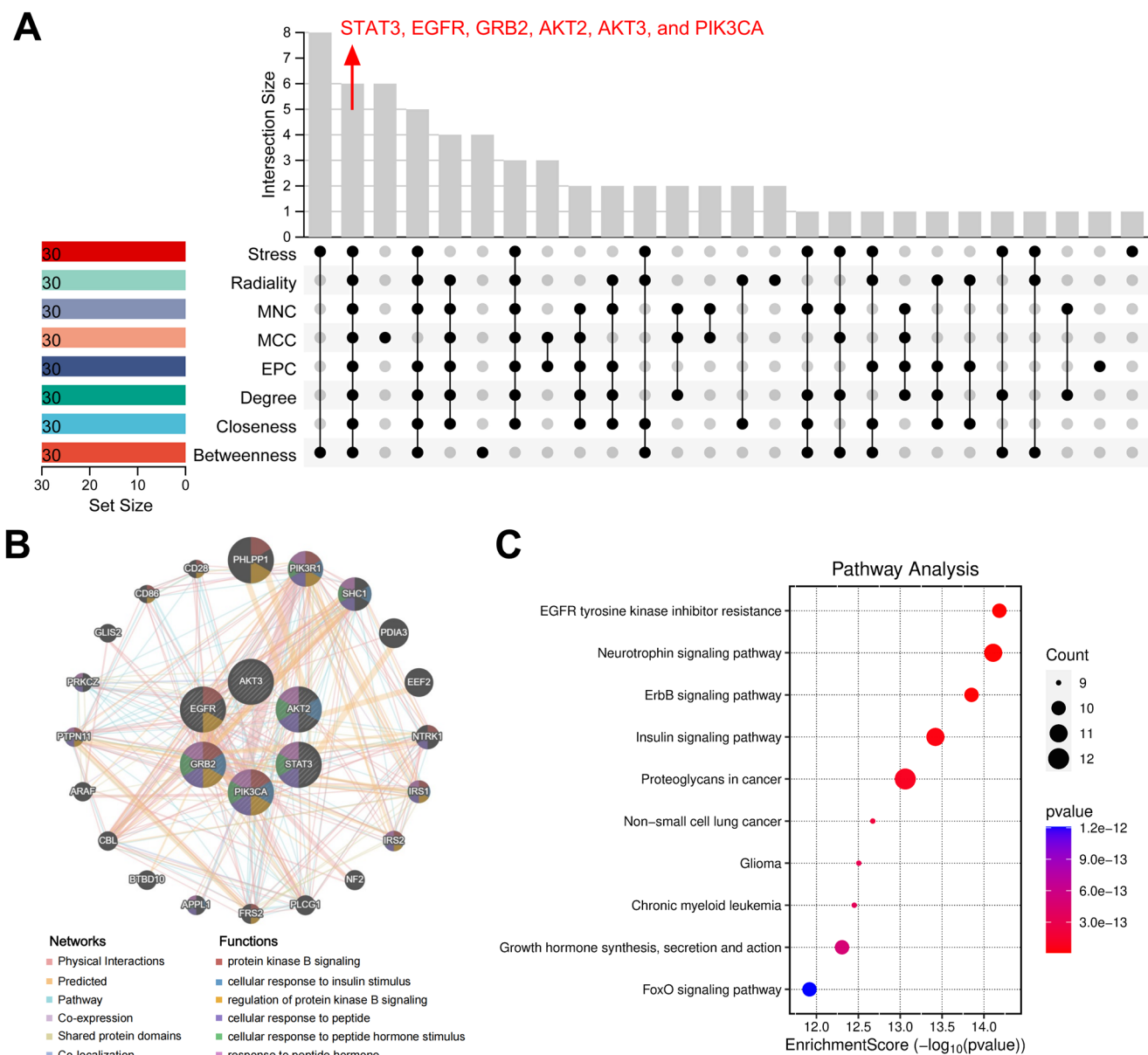


Figure 5. Co-expression network and enrichment analysis of hub genes. (A) Six hub genes were obtained with eight algorithms via cytoHubba plug-in. (B) The co-expression network of hub genes was established by GeneMANIA. (C) Bubble map of KEGG enrichment analysis. The horizontal axis is the enrichment score, and the vertical axis is the item name, and the bubble color represents the p value, and the bubble size represents the gene count.

Table 4. Summary of six hub genes.

No.	Targets	Uniprot ID	Full name	Betweenness	Closeness	Degree	EPC	MCC	MNC	Radiality
1	STAT3	P40763	Signal transducer and activator of transcription 3	6395.92943	89.04642857	28	46.383	3364	26	10.1614198
2	EGFR	P00533	Epidermal growth factor receptor	2910.09551	82.52738095	23	45.446	179,988	21	10.00570627
3	GRB2	P62993	Growth factor receptor-bound protein 2	2042.645313	75.17142857	20	41.41	6279	17	9.71652401
4	AKT2	P31751	RAC-beta serine/threonine-protein kinase	1417.393808	82.56309524	23	44.116	5602	23	10.01015523
5	AKT3	Q9Y243	RAC-gamma serine/threonine-protein kinase	1417.393808	82.56309524	23	44.147	5602	23	10.01015523
6	PIK3CA	P42336	Phosphatidylinositol 4,5-bisphosphate 3-kinase catalytic subunit alpha isoform	1118.921708	82.16309524	29	48.099	188,428	29	9.890033367

Note: EPC: edge percolated component; MCC: maximal clique centrality; MNC: maximum neighborhood component.

acid residues ARG-269, GLN-79 and THR-197 of AKT2 protein; kidjolanin formed three hydrogen bonds with amino acid residues TYR-327 and ARG-86 of AKT2 protein; and AKT2 inhibitor CCT128930 could form two hydrogen bonds with amino acid residues THR-82 and GLU-299 of AKT2 protein (Figure 8(D)). K3OBD formed one hydrogen bond with amino

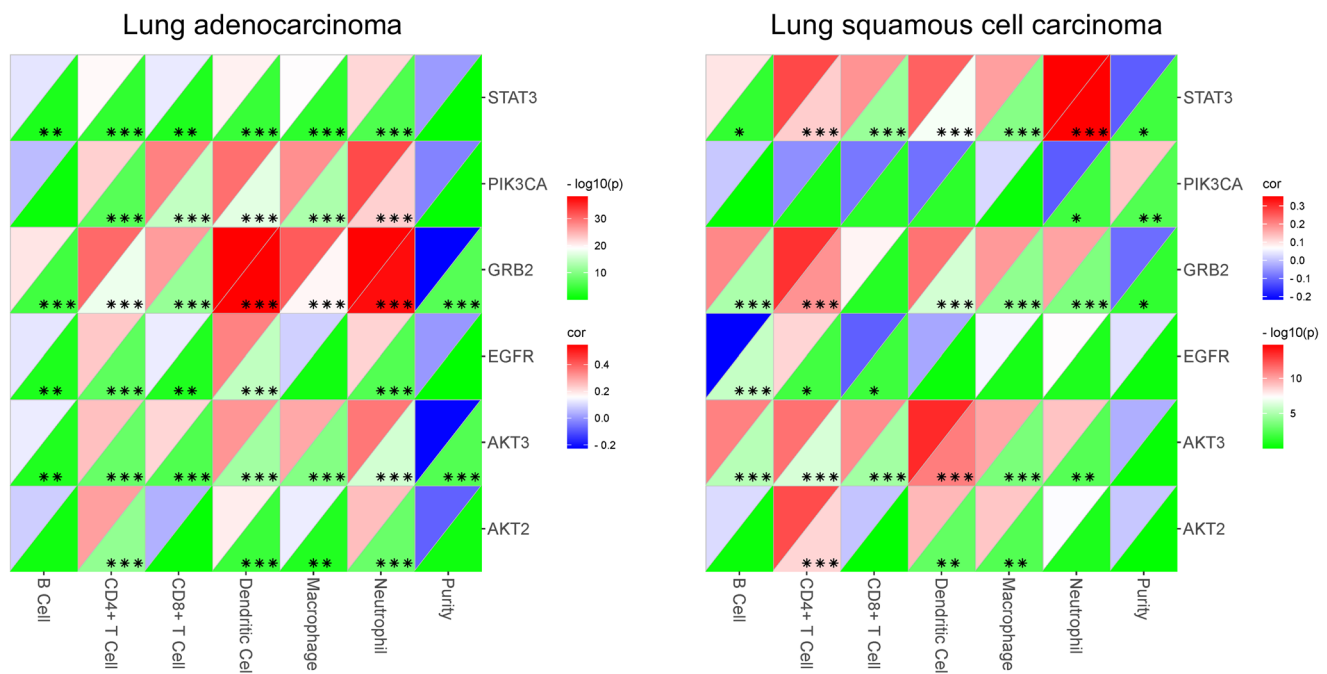


Figure 6. The relationship between hub gene expression and immune cell infiltration. A triangular heat map of correlation coefficients was used to visualize the correlation between hub genes (*STAT3*, *EGFR*, *GRB2*, *AKT2*, *AKT3* and *PIK3CA*) and different levels of immune cell infiltration. The horizontal axis represents different immune cells (B Cell, CD8+ T Cell, CD4+ T Cell, Macrophage, Neutrophil and Dendritic Cell). The vertical axis represents the hub genes. The correlation coefficients are shown in triangles of different colors. * $p < 0.05$, ** $p < 0.01$ and *** $p < 0.001$.

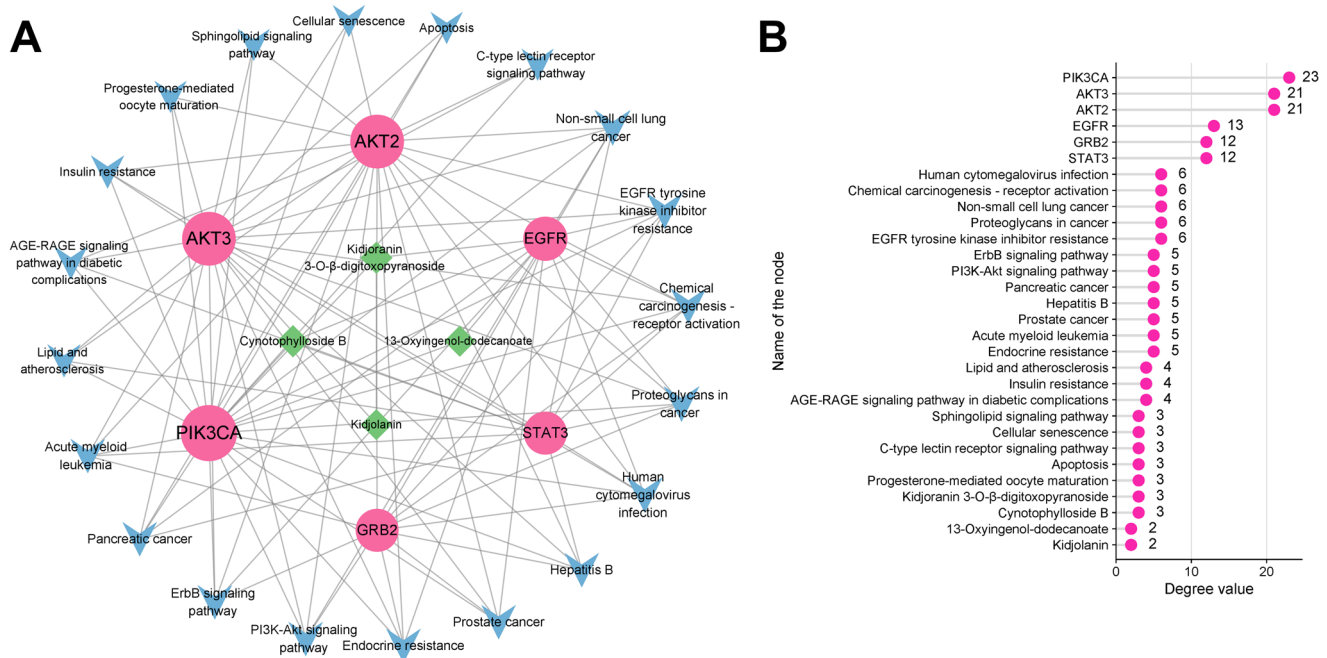


Figure 7. Construction and analysis of 'component-hub gene-pathway' network. (A) 'Component-hub gene-pathway' network. The pink circular nodes represent hub genes; blue V-shaped nodes represent pathways; and green diamond nodes represent components. The size of the node is proportional to degree value. (B) Statistical graph of degree value of the 'component - hub gene - pathway' network.

acid residues LYS-41 of *AKT3* protein; CB formed three hydrogen bonds with amino acid residues ARG-15 and THR-86 of *AKT3* protein; 13OD formed five hydrogen bonds with amino acid residues LEU-51, ARG-25, GLU-17 and TYR-18 of *AKT3* protein; kidjolanin formed two hydrogen bonds with amino acid residues GLU-17 and THR-86 of *AKT3* protein, and *AKT3* inhibitor AT7867 formed two hydrogen bonds with amino acid residues GLU-17 and GLY-16 of *AKT3* protein (Figure 8(E)). K3OBD formed three hydrogen bonds with amino acid residues

ARG-852, LYS-924 and ARG-818 of *PIK3CA* protein; CB formed four hydrogen bonds with amino acid residues LYS-924, ARG-852, GLU-849 and GLU-172 of *PIK3CA* protein; 13OD formed three hydrogen bonds with amino acid residues ASN-756, ASN-170 and GLN-630 of *PIK3CA* protein; kidjolanin formed four hydrogen bonds with amino acid residues LYS-924, MET-833, GLU-821 and ARG-818 of *PIK3CA* protein; and the *PIK3CA* inhibitor dactolisib could form four hydrogen bonds with amino acid residues SER-774 and SER-854 of *PIK3CA* protein (Figure 8(F)). As

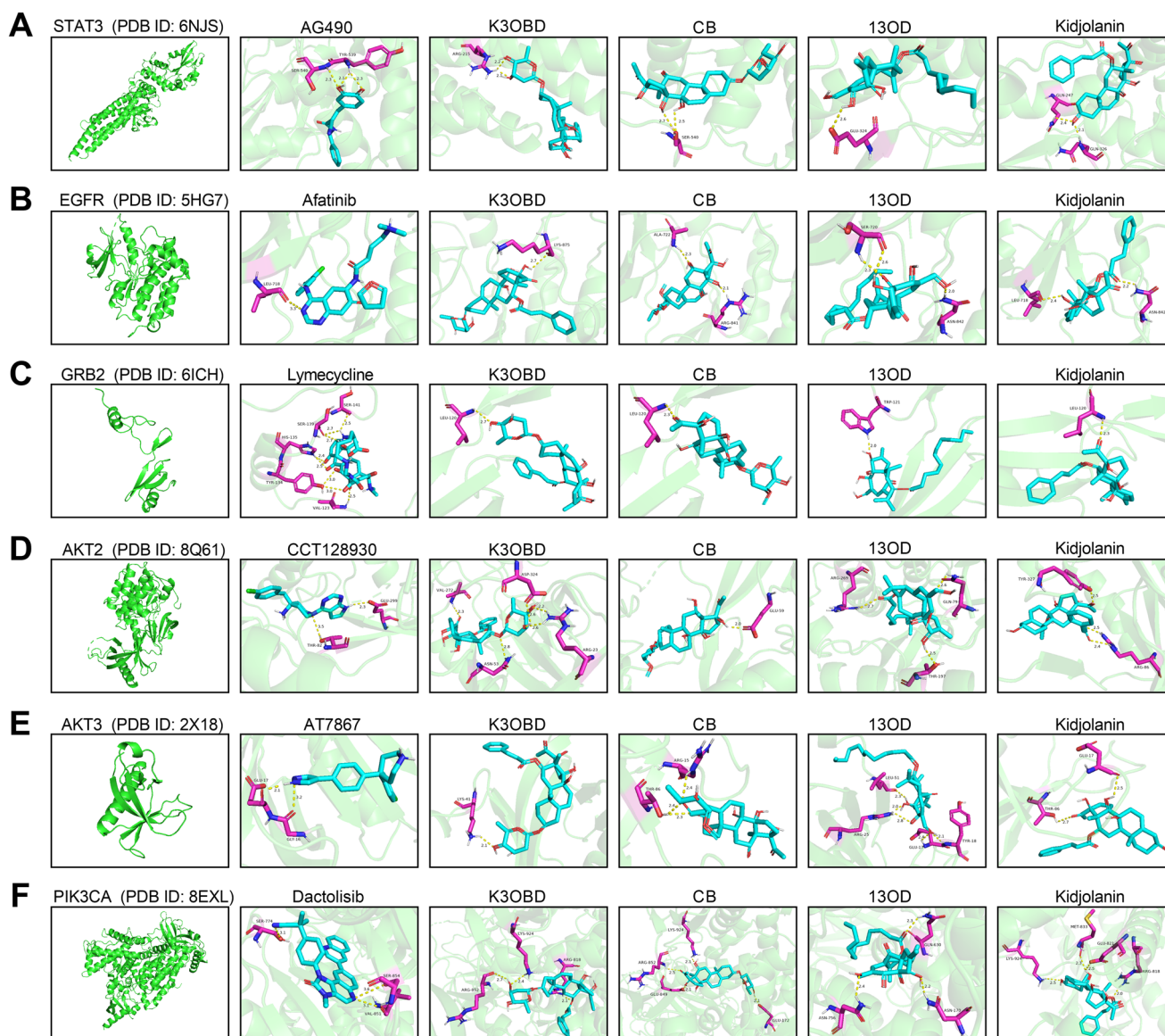


Figure 8. Molecular docking diagram of key components of gansui and hub target proteins. (A–F) Molecular docking 3D diagram of *STAT3* (A), *EGFR* (B), *GRB2* (C), *AKT2* (D), *AKT3* (E), *PIK3CA* (F) proteins and key components and hub protein inhibitors. Green represents macromolecules; blue represents ligands; purple represents amino acid residues around the binding bag; yellow dashed lines represent hydrogen bonds.

shown in Table 5, it was found that the binding affinities between key compounds of Gansui (K3OBD, CB, 13OD and kidjolanin) and hub proteins (*STAT3*, *EGFR*, *GRB2*, *AKT2*, *AKT3* and *PIK3CA*) were all less than -5 kcal/mol. Interestingly, some components of Gansui showed better binding affinities with the hub targets compared with the known inhibitors. A recent study has reported that 13OD inhibits the growth of NSCLC cells by targeting Unc-51 like autophagy activating kinase 1 (*ULK1*) (Wang et al. 2024). We found that K3OBD, CB, 13OD and kidjolanin could form hydrogen bonds with *ULK1* protein (PDB ID: 6MNH) with a binding affinity of less than -5 kcal/mol. However, the binding affinity between *ULK1* protein inhibitor (inlexisertib) and *ULK1* protein was greater than the binding affinity between key components and *ULK1* (Figure 9).

In vitro validation of kidjolanin's anti-NSCLC effect

To clarify the effect of Gansui on the viability of NSCLC cells, the effects of kidjolanin on A549 and NCI-H1385

cells were examined at different concentrations (0, 20, 40, 60, 80, 100 μ M). The results showed that kidjolanin significantly decreased the viability of A549 and NCI-H1385 cells in a dose-dependent manner (Figure 10(A)). The IC_{50} values for A549 and NCI-H1385 cells were 58.19 μ M and 55.71 μ M, respectively, indicating that kidjolanin had significant anti-NSCLC effects. Consistently, flow cytometry showed that kidjolanin could promote apoptosis of A549 and NCI-H1385 cells (Figure 10(B)). In addition, the effects of kidjolanin on mRNA expression levels of hub genes were detected by qRT-PCR. Interestingly, the results showed that kidjolanin could significantly reduce the expression of *STAT3*, *EGFR*, *GRB2*, *AKT2*, *AKT3* and *PIK3CA* mRNA in A549 and NCI-H1385 cells in a dose-dependent manner (Figure 10(C–H)), suggesting Gansui could not only reduce the activity of these proteins, but also modulate the expression level of these targets. These results suggest that the kidjolanin can inhibit the viability of NSCLC cells by acting on hub targets such as *STAT3*, *EGFR*, *GRB2*, *AKT2*, *AKT3* and *PIK3CA*.

Table 5. The binding energy between the key active ingredients of Gansui and the main hub target genes.

	Compound	Binding affinity (kcal/mol)	Interactions	Residues
STAT3 (6NJS)	K3OBD	-7.9	2 H-bonds	ARG-215
	CB	-7.6	2 H-bonds	SER-540
	13OD	-6.3	1 H-bond	GLU-324
	Kidjolanin	-7.8	2 H-bonds	GLN-326
				GLN-247
EGFR (5HG7)	AG490	-7.0	3 H-bonds	SER-540
				TYR-539
	K3OBD	-9.4	1 H-bond	LYS-875
	CB	-8.6	2 H-bonds	ALA-722
				ARG-841
GRB2 (6ICH)	13OD	-7.6	3 H-bonds	SER-720
				ASN-842
	Kidjolanin	-8.5	2 H-bonds	ASN-842
				LEU-718
	Afatinib	-8.3	1 H-bond	LEU-718
	K3OBD	-7.7	1 H-bond	LEU-120
	CB	-7.0	1 H-bond	LEU-120
	13OD	-7.1	1 H-bond	TRP-121
	Kidjolanin	-8.3	1 H-bond	LEU-120
	Lymecycline	-5.9	8 H-bonds	VAL-123
AKT2 (8Q61)				TYR-134
				HIS-135
				SER-139
				SER-141
	K3OBD	-9.7	5 H-bonds	VAL-272
				ASN-53
				ARG-23
	CB	-8.1	1 H-bond	ASP-324
	13OD	-7.5	3 H-bonds	GLU-59
				ARG-269
				GLN-79
	Kidjolanin	-8.4	3 H-bonds	THR-197
				TYR-327
				ARG-86
	CCT128930	-8.9	2 H-bonds	THR-82
AKT3 (2×18)				GLU-299
	K3OBD	-8.7	1 H-bond	LYS-41
	CB	-7.1	3 H-bonds	ARG-15
				THR-86
	13OD	-6.3	5 H-bonds	LEU-51
				ARG-25
				GLU-17
				TYR-18
	Kidjolanin	-7.7	2 H-bonds	GLU-17
				THR-86
	AT7867	-6.6	2 H-bonds	GLU-17
				GLY-16
PIK3CA (8EXL)	K3OBD	-10.0	3 H-bonds	ARG-852
				LYS-924
	CB	-9.2	4 H-bonds	ARG-818
				LYS-924
				ARG-852
				GLU-849
	13OD	-7.1	3 H-bonds	GLU-172
				ASN-756
				ASN-170
	Kidjolanin	-9.2	4 H-bonds	GLN-630
				LYS-924
				MET-833
				GLU-821
				ARG-818
	Dactolisib	-11.3	3 H-bonds	SER-774
				SER-854
				VAL-851

Note: K3OBD: kidjoranin 3-O- β -digitoxopyranoside; CB: cynotophylloside B; 13OD: 13-Oxyingenol-dodecanoate.

Kidjolanin can enhance paclitaxel-induced proliferation inhibition and apoptosis of NSCLC cells

To detect the effect of kidjolanin on paclitaxel-induced proliferation inhibition, we treated A549 and NCI-H1385 cells with different concentrations (0, 1.25, 2.5, 5, 10 and 20 μ g/mL) of paclitaxel (Figure 11(A)) in the presence or absence of 60 μ M

kidjolanin. Compared with the group without kidjolanin treatment, the viability of A549 and NCI-H1385 cells in the kidjolanin treatment group was significantly reduced (Figure 11(B)). In the absence of kidjolanin treatment, the IC₅₀ of paclitaxel for A549 and NCI-H1385 cells were 11.03 μ g/mL and 11.54 μ g/mL, respectively; in the presence of kidjolanin treatment, the IC₅₀ of paclitaxel for A549 and NCI-H1385 cells were 4.624 μ g/mL and

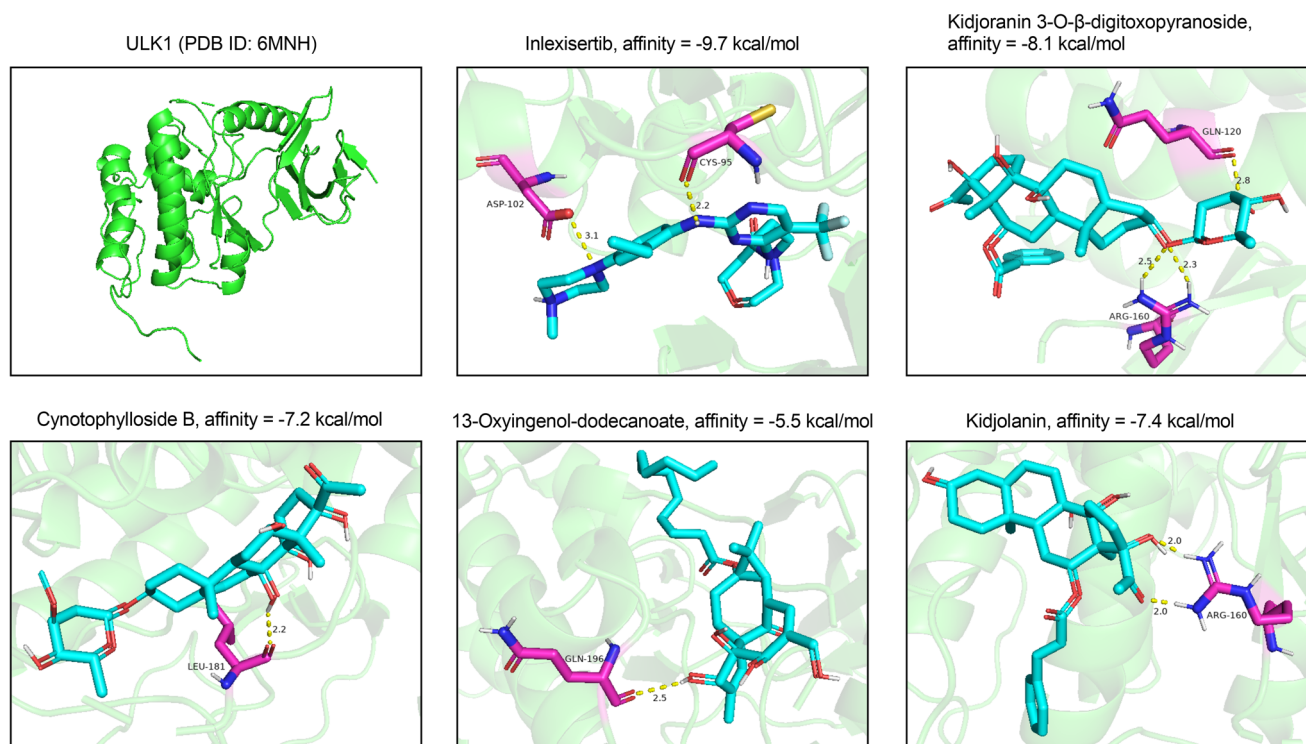


Figure 9. 3D Molecular docking diagram of ULK1 protein with its inhibitor (inlxisetib) and key components of gansui (kidjolanin 3-O- β -digitoxopyranoside, cynophylloside B, 13-oxyingenol dodecanoate and kidjolanin). Green represents ULK1 protein; blue represents ligand; purple represents the amino acid residues around the binding bag; the yellow dashed line represents hydrogen bonds.

5.129 $\mu\text{g/mL}$, respectively (Figure 11(B)). Flow cytometry results showed that paclitaxel significantly induced apoptosis of A549 and NCI-H1385 cells, and the apoptosis induced by paclitaxel was further enhanced by kidjolanin (Figure 11(C)). These results indicate that Gansui may sensitize NSCLC cells to chemotherapeutics.

Discussion

Despite great progress in understanding tumor heterogeneity and molecular structure of tumor cells, therapeutic resistance and side effects of current drugs remain major obstacles (Gu et al. 2023). Traditional Chinese medicine plays a unique role in the alternative treatment of NSCLC (Xu et al. 2019). It has been reported that the main active components of Gansui (diterpenoids and triterpenoids) have anti-proliferation activities against various human malignancies such as lung cancer and liver cancer (Ma et al. 2016). However, the mechanism of action of Gansui in the treatment of NSCLC has not been systematically studied.

Based on network pharmacological analysis, we found that Gansui contained at least 16 active ingredients corresponding to 337 targets, of which 298 targets overlapped with the genes associated with NSCLC. These 298 targets were considered as potential target genes for the treatment of NSCLC with Gansui. GO-BP analysis showed that the 298 genes were mainly responsible for peptidyl-serine phosphorylation, peptidyl-serine modification, rhythmic process, regulation of small molecule metabolic process and positive regulation of protein transport. In addition, KEGG analysis of candidate targets showed that the mechanism of Gansui therapy in NSCLC may be related to the pathways associated with endocrine resistance, acute myeloid leukemia, AGE-RAGE signaling pathway in diabetic complications, prostate

cancer, insulin resistance, progesterone-mediated oocyte maturation, EGFR tyrosine kinase inhibitor resistance, apoptosis, proteoglycans in cancer, hepatitis B. PPI network analysis showed that *STAT3*, *EGFR*, *GRB2*, *AKT2*, *AKT3* and *PIK3CA* were hub targets for Gansui against NSCLC. These hub genes are mainly associated with EGFR pathway. Reportedly, activation of the EGFR pathway promotes the proliferation of NSCLC cells and is associated with chemotherapy resistance (Wu et al. 2021). In addition, targeted therapy targeting the EGFR pathway has become one of the important means of treating NSCLC (He J et al. 2021). Therefore, we suppose that the regulation of EGFR pathway may be a potential mechanism for the treatment of NSCLC by Gansui.

STAT3 is an important transcription factor that is abnormally activated in NSCLC and is associated with poor clinical prognosis (Xu and Lu 2014). *EGFR* mutations are closely related to the occurrence and development of NSCLC (Harrison et al. 2020). Targeted therapy targeting *EGFR*, such as *EGFR*-tyrosine kinase inhibitors (TKIs), has become an important approach of treating *EGFR* mutation-positive NSCLC patients (Remon et al. 2018). *GRB2* can promote the proliferation and survival of NSCLC cells while enhancing their resistance to chemotherapy drugs (Wang et al. 2015; Xu et al. 2016). *AKT2* and *AKT3* are members of the AKT family and play important roles in the development of NSCLC (Zhou et al. 2010). Overexpression of *AKT2* is associated with poor prognosis in NSCLC patients (Liu et al. 2020). In NSCLC, activation of *AKT3* can promote tumor growth and the development of drug resistance (Xu et al. 2022). *PIK3CA* gene mutations are common in NSCLC. *PIK3CA* mutations can enhance the activation of the PI3K/AKT pathway, promoting NSCLC cell survival and proliferation (He Y et al. 2021), and this mechanism also impairs the effectiveness of *EGFR*-TKIs (Liu et al. 2024). In the present work, *in vitro* experiments showed that kidjolanin could significantly reduce the viability of NSCLC

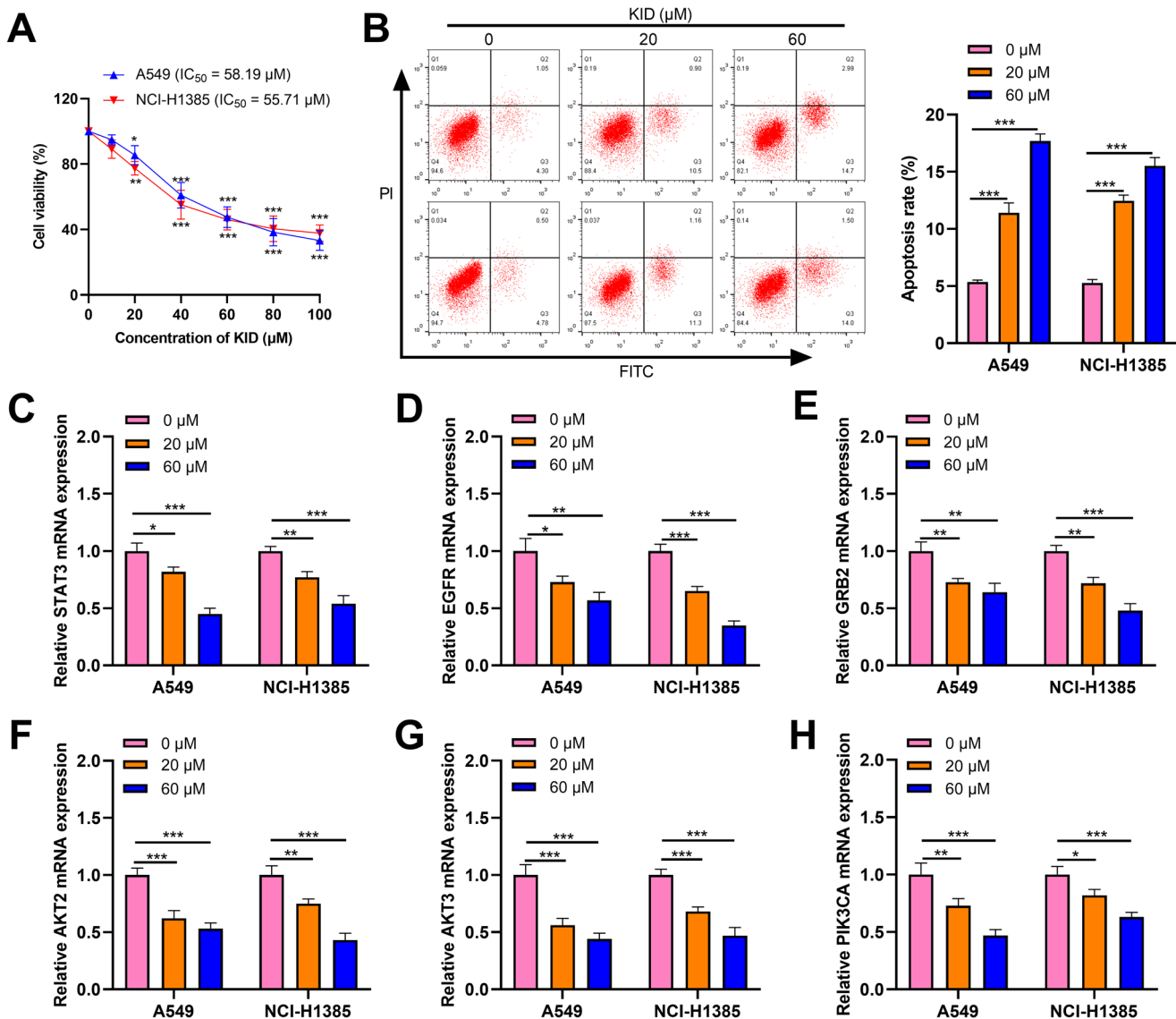


Figure 10. Kidjanolin inhibited NSCLC cell viability, as well as the expression levels of hub targets. (A) A549 and NCI-H1385 cells were treated with different concentrations of kidjanolin (0, 20, 40, 60, 80, 100 μM), and cell viability was detected by CCK-8 assay. (B) The apoptosis of A549 and NCI-H1385 cells treated with different concentrations of kidjanolin (0, 20 and 60 μM) was detected by flow cytometry. (C–H) After treating A549 and NCI-H1385 cells with different concentrations of kidjanolin (0, 20 and 60 μM) for 24 h, the mRNA expression levels of *STAT3* (C), *EGFR* (D), *GRB2* (E), *AKT2* (F), *AKT3* (G) and *PIK3CA* (H) were detected by qRT-PCR. KID: kidjanolin. * $p < 0.05$, ** $p < 0.01$, *** $p < 0.001$.

cells, promote cell apoptosis and inhibit the mRNA expression levels of *STAT3*, *EGFR*, *GRB2*, *AKT2*, *AKT3* and *PIK3CA*. Considering the hub targets are significantly associated with drug resistance of NSCLC cells, our data suggest that Gansui extract is promising to sensitize NSCLC cells to anti-cancer treatment. As expected, the inhibition of proliferation and apoptosis of NSCLC cells induced by paclitaxel could be enhanced by kidjanolin. Of course, it is intriguing to explore the tumor-suppressive properties of other crucial components of Gansui, and whether Gansui extract enhances the sensitivity of NSCLC cells to TKIs in the following work. Additionally, it was revealed the expression of *STAT3*, *EGFR*, *GRB2*, *AKT2*, *AKT3* and *PIK3CA* was positively correlated with the infiltration abundance of CD4⁺T cells, neutrophil and dendritic cells in LUAD; in LUSC, the expression of *STAT3*, *EGFR*, *GRB2*, *AKT2* and *AKT3* was positively correlated with the abundance of CD4⁺T cells infiltration. This suggests that these hub genes may be involved in the remodeling of immune microenvironment of NSCLC, and Gansui extract may also promote the effectiveness

of immunotherapy, which remains to be validated with animal models in the future.

STAT3, *EGFR*, *GRB2*, *AKT2*, *AKT3* and *PIK3CA* had considerable binding affinities with key components of Gansui, including K3OBD, CB, 13OD and kidjanolin. Compared to their inhibitors such as AG490, afatinib, lymecycline and AT7867, the crucial components of Gansui even showed higher binding affinities. Molecular docking in the present work, showed that K3OBD, CB, 13OD and kidjanolin mainly bound with DNA binding domain and linker domain of *STAT3*, suggesting these components could probably modulate the structure and transcription-regulating function of *STAT3*. All of K3OBD, CB, 13OD and kidjanolin could bind with intracellular tyrosine kinase domain of *EGFR* and SH2 domain of *GRB2* (which interacts with *EGFR* to be phosphorylated), suggesting these components probably block the phosphorylation of *EGFR* and downstream signal transduction. For *AKT2* and *AKT3*, the bioactive components of Gansui mainly bound with N-terminal PH domain, which is

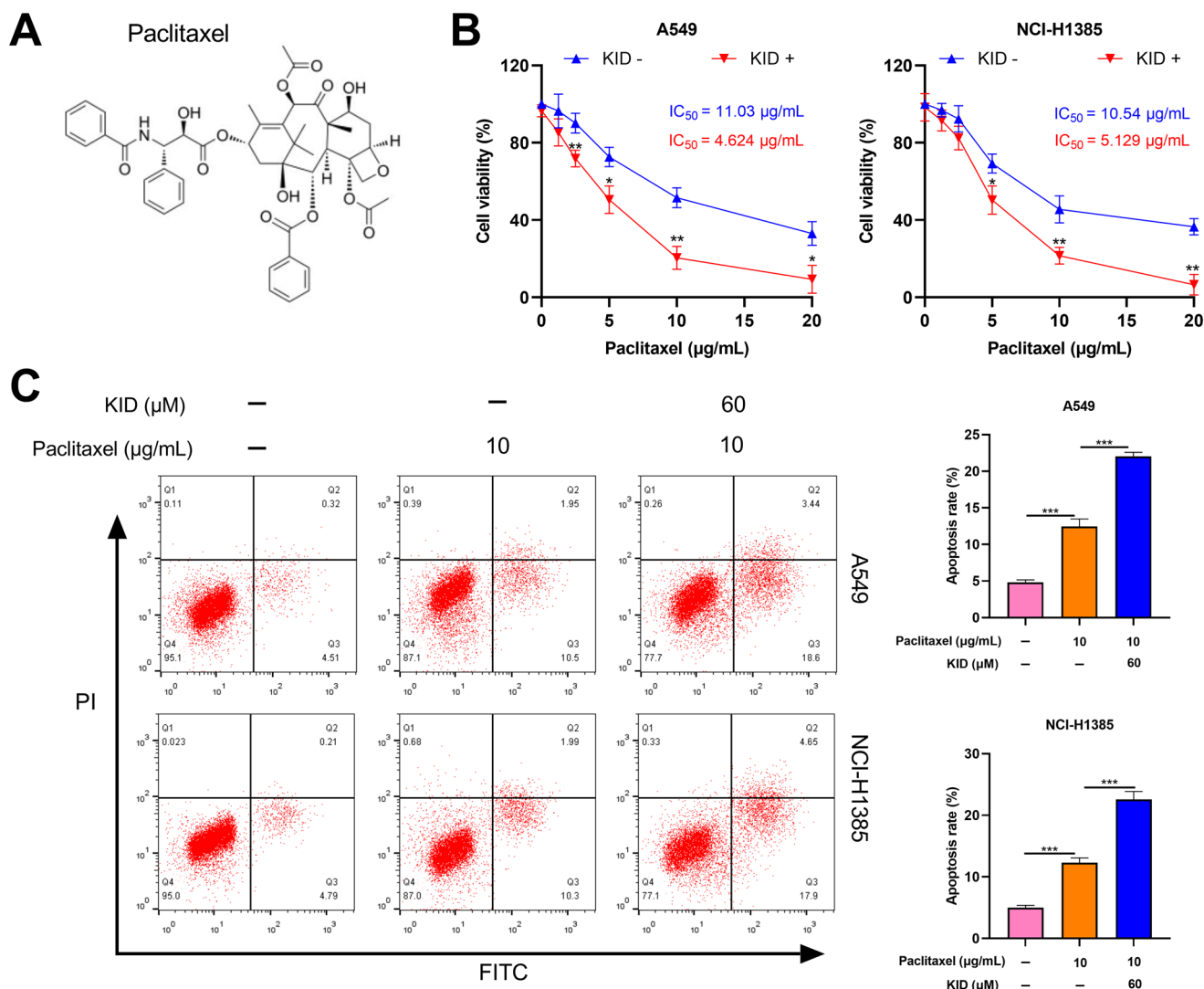


Figure 11. Kidjolanin enhanced proliferation inhibition and apoptosis of NSCLC cells induced by paclitaxel. (A) A549 and NCI-H1385 cells were treated with different concentrations (0, 1.25, 2.5, 5, 10 and 20 $\mu\text{g/mL}$) of paclitaxel for 48 h, with or without treatment with 60 μM kidjolanin. Then, the CCK-8 method was used to detect cell viability. (B,C) A549 and NCI-H1385 cells were treated with 10 $\mu\text{g/mL}$ paclitaxel or/and 60 μM kidjolanin, and apoptosis was detected by flow cytometry. KID: kidjolanin. * $p < 0.05$, ** $p < 0.01$, *** $p < 0.001$.

important in mediating locating AKT in cytomembrane. For PIK3CA, K3OBD, CB and kidjolanin could probably bind with its kinase domain and block signal transduction. All of these findings imply that Gansui extract may block signal transduction of multiple pivotal pathways in cancer biology, which remain to be validated with more biochemical experiments.

Conclusions

STAT3, EGFR, GRB2, AKT2, AKT3 and PIK3CA are potential targets of Gansui. Gansui may be a potential candidate drug for the treatment of NSCLC, and its therapeutic effect may be related to its key components K3OBD, CB, 13OD and kidjolanin.

Authors contributions

Conceived and designed the experiments: WLL; performed the experiments: XXY and WLL; analyzed the data: XXY; wrote the paper: WLL and XXY. All authors read and approved the final manuscript.

Disclosure statement

No potential conflict of interest was reported by the author(s).

Funding

This study was supported by Fundamental Research Funds in Universities of Heilongjiang Province (2024-KYYWF-1023), Key R&D Program Project of Heilongjiang Province (2022ZX02C08).

Data availability statement

The data used to support the findings of this study are available from the corresponding author upon request.

References

- Cheng F, Yang Y, Zhang L, Cao Y, Yao W, Tang Y, Ding A. 2015. A natural triterpene derivative from *Euphorbia kansui* inhibits cell proliferation and induces apoptosis against rat intestinal epithelioid cell line *in vitro*. *Int J Mol Sci*. 16(8):18956–18975. doi: 10.3390/ijms160818956.

- Feng X, Li J, Li H, Chen X, Liu D, Li R. 2023. Bioactive C21 steroidal glycosides from *Euphorbia kansui* promoted HepG2 cell apoptosis via the degradation of ATP1A1 and inhibited macrophage polarization under co-cultivation. *Molecules*. 28(6):2830. doi: [10.3390/molecules28062830](https://doi.org/10.3390/molecules28062830).
- Gu L, Li Z, Zhang X, Chen M, Zhang X. 2023. Identification of MAP Kinase Kinase 3 as a protein target of myricetin in non-small cell lung cancer cells. *Biomed Pharmacother*. 161:114460. doi: [10.1016/j.biopha.2023.114460](https://doi.org/10.1016/j.biopha.2023.114460).
- Harrison PT, Vyse S, Huang PH. 2020. Rare epidermal growth factor receptor (EGFR) mutations in non-small cell lung cancer. *Semin Cancer Biol*. 61:167–179. doi: [10.1016/j.semcancer.2019.09.015](https://doi.org/10.1016/j.semcancer.2019.09.015).
- He J, Huang Z, Han L, Gong Y, Xie C. 2021. Mechanisms and management of 3rd-generation EGFR-TKI resistance in advanced non-small cell lung cancer (review). *Int J Oncol*. 59(5):90. doi: [10.3892/ijo.2021.5270](https://doi.org/10.3892/ijo.2021.5270).
- He Y, Sun MM, Zhang GG, Yang J, Chen KS, Xu WW, Li B. 2021. Targeting PI3K/Akt signal transduction for cancer therapy. *Signal Transduct Target Ther*. 6(1):425. doi: [10.1038/s41392-021-00828-5](https://doi.org/10.1038/s41392-021-00828-5).
- Herbst RS, Morgensztern D, Boshoff C. 2018. The biology and management of non-small cell lung cancer. *Nature*. 553(7689):446–454. doi: [10.1038/nature25183](https://doi.org/10.1038/nature25183).
- Li X, Qin H, Anwar A, Zhang X, Yu F, Tan Z, Tang Z. 2022. Molecular mechanism analysis of m6A modification-related lncRNA-miRNA-mRNA network in regulating autophagy in acute pancreatitis. *Islets*. 14(1):184–199. doi: [10.1080/19382014.2022.2132099](https://doi.org/10.1080/19382014.2022.2132099).
- Liu T, Zhu J, Du W, Ning W, Zhang Y, Zeng Y, Liu Z, Huang JA. 2020. AKT2 drives cancer progression and is negatively modulated by miR-124 in human lung adenocarcinoma. *Respir Res*. 21(1):227. doi: [10.1186/s12931-020-01491-0](https://doi.org/10.1186/s12931-020-01491-0).
- Liu X, Mei W, Zhang P, Zeng C. 2024. PIK3CA mutation as an acquired resistance driver to EGFR-TKIs in non-small cell lung cancer: clinical challenges and opportunities. *Pharmacol Res*. 202:107123. doi: [10.1016/j.phrs.2024.107123](https://doi.org/10.1016/j.phrs.2024.107123).
- Long X, Liu L, Zhao Q, Xu X, Liu P, Zhang G, Lin J. 2022. Comprehensive analysis of tripterine anti-ovarian cancer effects using weighted gene co-expression network analysis and molecular docking. *Med Sci Monit*. 28:e932139. doi: [10.12659/MSM.932139](https://doi.org/10.12659/MSM.932139).
- Lu T, Yang X, Huang Y, Zhao M, Li M, Ma K, Yin J, Zhan C, Wang Q. 2019. Trends in the incidence, treatment, and survival of patients with lung cancer in the last four decades. *Cancer Manag Res*. 11:943–953. doi: [10.2147/CMAR.S187317](https://doi.org/10.2147/CMAR.S187317).
- Ma H, Yang S, Lu H, Zhang Y. 2016. Bioassay-guided separation of anti-tumor components from *Euphorbia kansui* by means of two-dimensional preparative high performance liquid chromatography and real-time cell analysis. *Anal Sci*. 32(5):581–586. doi: [10.2116/analsci.32.581](https://doi.org/10.2116/analsci.32.581).
- Qian Y, Yi F. 2024. Inulae Flos is a potential herbal medicine to treat glioma: a study based on gene expression profile analysis, network pharmacology and molecular docking. *Diagn Ther*. 3(1):32–52.
- Remon J, Steuer CE, Ramalingam SS, Felip E. 2018. Osimertinib and other third-generation EGFR TKI in EGFR-mutant NSCLC patients. *Ann Oncol*. 29(suppl_1):i20–i27. doi: [10.1093/annonc/mdx704](https://doi.org/10.1093/annonc/mdx704).
- Shen J, Kai J, Tang Y, Zhang L, Su S, Duan JA. 2016. The chemical and biological properties of *Euphorbia kansui*. *Am J Chin Med*. 44(2):253–273. doi: [10.1142/S0192415X16500154](https://doi.org/10.1142/S0192415X16500154).
- Soerjomataram I, Bray F. 2021. Planning for tomorrow: global cancer incidence and the role of prevention 2020–2070. *Nat Rev Clin Oncol*. 18(10):663–672. doi: [10.1038/s41571-021-00514-z](https://doi.org/10.1038/s41571-021-00514-z).
- Sun H, Wang H, Shi L, Wang M, Li J, Shi J, Ni M, Hu X, Chen Y. 2020. Physician preferences for chemotherapy in the treatment of non-small cell lung cancer in China: evidence from multicentre discrete choice experiments. *BMJ Open*. 10(2):e032336. doi: [10.1136/bmjopen-2019-032336](https://doi.org/10.1136/bmjopen-2019-032336).
- Sung H, Ferlay J, Siegel RL, Laversanne M, Soerjomataram I, Jemal A, Bray F. 2021. Global cancer statistics 2020: GLOBOCAN estimates of incidence and mortality worldwide for 36 cancers in 185 countries. *CA Cancer J Clin*. 71(3):209–249. doi: [10.3322/caac.21660](https://doi.org/10.3322/caac.21660).
- Wang WJ, Mou K, Wu XF, Zhang JZ, Ren G, Qi JD, Xu YF, Yao X. 2015. Grb2-associated binder 2 silencing impairs growth and migration of H1975 cells via modulation of PI3K-Akt signaling. *Int J Clin Exp Pathol*. 8(9):10575–10584.
- Wang XY, Wang YJ, Guo BW, Hou ZL, Zhang GX, Han Z, Liu Q, Yao GD, Song SJ. 2024. 13-Oxyingenol-dodecanoate inhibits the growth of non-small cell lung cancer cells by targeting ULK1. *Bioorg Chem*. 147:107367. doi: [10.1016/j.bioorg.2024.107367](https://doi.org/10.1016/j.bioorg.2024.107367).
- Wang Y, Zhang Y, Wang Y, Shu X, Lu C, Shao S, Liu X, Yang C, Luo J, Du Q. 2021. Using network pharmacology and molecular docking to explore the mechanism of Shan Ci Gu (*Cremastra appendiculata*) against non-small cell lung cancer. *Front Chem*. 9:682862. doi: [10.3389/fchem.2021.682862](https://doi.org/10.3389/fchem.2021.682862).
- Wei W, Zeng H, Zheng R, Zhang S, An L, Chen R, Wang S, Sun K, Matsuda T, Bray F, et al. 2020. Cancer registration in China and its role in cancer prevention and control. *Lancet Oncol*. 21(7):e342–e349. doi: [10.1016/S1470-2045\(20\)30073-5](https://doi.org/10.1016/S1470-2045(20)30073-5).
- Wu S, Luo M, To KKW, Zhang J, Su C, Zhang H, An S, Wang F, Chen D, Fu L. 2021. Intercellular transfer of exosomal wild type EGFR triggers osimertinib resistance in non-small cell lung cancer. *Mol Cancer*. 20(1):17. doi: [10.1186/s12943-021-01307-9](https://doi.org/10.1186/s12943-021-01307-9).
- Xiang C, Liao Y, Chen Z, Xiao B, Zhao Z, Li A, Xia Y, Wang P, Li H, Xiao T. 2022. Network pharmacology and molecular docking to elucidate the potential mechanism of ligusticum chuanxiong against osteoarthritis. *Front Pharmacol*. 13:854215. doi: [10.3389/fphar.2022.854215](https://doi.org/10.3389/fphar.2022.854215).
- Xu F, Zhang X, Chen Z, He S, Guo J, Yu L, Wang Y, Hou C, Ai-Furas H, Zheng Z, et al. 2022. Discovery of isoform-selective Akt3 degraders overcoming osimertinib-induced resistance in non-small cell lung cancer cells. *J Med Chem*. 65(20):14032–14048. doi: [10.1021/acs.jmedchem.2c01246](https://doi.org/10.1021/acs.jmedchem.2c01246).
- Xu LJ, Wang YC, Lan HW, Li J, Xia T. 2016. Grb2-associated binder-2 gene promotes migration of non-small cell lung cancer cells via Akt signaling pathway. *Am J Transl Res*. 8(2):1208–1217.
- Xu YH, Lu S. 2014. A meta-analysis of STAT3 and phospho-STAT3 expression and survival of patients with non-small-cell lung cancer. *Eur J Surg Oncol*. 40(3):311–317. doi: [10.1016/j.ejso.2013.11.012](https://doi.org/10.1016/j.ejso.2013.11.012).
- Xu Z, Zhang F, Zhu Y, Liu F, Chen X, Wei L, Zhang N, Zhou Q, Zhong H, Yao C, et al. 2019. Traditional Chinese medicine Ze-Qi-Tang formula inhibit growth of non-small-cell lung cancer cells through the p53 pathway. *J Ethnopharmacol*. 234:180–188. doi: [10.1016/j.jep.2019.01.007](https://doi.org/10.1016/j.jep.2019.01.007).
- Zhang C, Wu W, Yang J, Sun J. 2022. Application of artificial intelligence in respiratory medicine. *JDH*. 1(1):30–39. doi: [10.55976/jdh.1202215330-39](https://doi.org/10.55976/jdh.1202215330-39).
- Zhang Q, Zhang Y, Zhou SK, Wang K, Zhang M, Chen PD, Yao WF, Tang YP, Wu JH, Zhang L. 2019. Toxicity reduction of *Euphorbia kansui* stir-fried with vinegar based on conversion of 3-O-(2'E,4'Z-decadi-enoyl)-20-O-acetylengenol. *Molecules*. 24(20):3806. doi: [10.3390/molecules24203806](https://doi.org/10.3390/molecules24203806).
- Zhang Q, Zhou QR, Lou JW, Chen PD, Yao WF, Tao WW, Tang YP, Dai GC, Wang K, Zhang L. 2017. Chemical constituents from *Euphorbia kansui*. *Molecules*. 22(12):2176. doi: [10.3390/molecules22122176](https://doi.org/10.3390/molecules22122176).
- Zhou B, Yang Y, Pang X, Shi J, Jiang T, Zheng X. 2023. Quercetin inhibits DNA damage responses to induce apoptosis via SIRT5/PI3K/AKT pathway in non-small cell lung cancer. *Biomed Pharmacother*. 165:115071. doi: [10.1016/j.biopha.2023.115071](https://doi.org/10.1016/j.biopha.2023.115071).
- Zhou F, Chang Z, Zhang L, Hong YK, Shen B, Wang B, Zhang F, Lu G, Tvorogov D, Alitalo K, et al. 2010. Akt/protein kinase B is required for lymphatic network formation, remodeling, and valve development. *Am J Pathol*. 177(4):2124–2133. doi: [10.2353/ajpath.2010.091301](https://doi.org/10.2353/ajpath.2010.091301).